Doctorate Dissertation (Censored)

博士論文 (要約)

A study on the background sea surface temperature field and moist processes contributing to the realization of the Madden-Julian Oscillation

(マッデン・ジュリアン振動の発生に寄与する海面水温背景場と湿潤過程の研究)

A Dissertation Submitted for Degree of Doctor of Philosophy

July 2018

平成３０年７月博士（理学）申請

Department of Earth and Planetary Science, Graduate School of Science,

The University of Tokyo

東京大学大学院理学系研究科地球惑星科学専攻

Tamaki Suematsu

末松　環

論文の内容の要旨

A study on the background sea surface temperature field and moist processes contributing to the realization of the Madden-Julian Oscillation

(マッデン・ジュリアン振動の発生に寄与する海面水温背景場と湿潤過程の研究)

氏名　末松　環

The Madden-Julian Oscillation (MJO) is prominent intraseasonal variability in the tropics which is now widely accepted to be an eastward proceeding envelope of convective activity coupled with circulation. However essential factors for the realization of the MJO and what modulates their properties are still controversial. This study hypothesizes that for an MJO-like large-scale atmospheric circulation to develop and to persist on an intraseasonal timescale, a background state longer than the intraseasonal timescale should provide long-standing conditions that support the development of MJO convection. Based on this hypothesis, I investigated for an environment favorable for the development of the MJO and analyzed how MJO properties are affected by the differences in the environment that they develop in.

An environment supporting MJO development was investigated by classifying MJO-like atmospheric patterns as MJO and regionally confined convective (RCC) events. Comparison of MJO and RCC events showed that even when preceded by a major convective suppression event, convective events did not develop into an MJO when the large-scale buildup of moist static energy (MSE) was inhibited. The difference in the MSE accumulation between MJO and RCC was related to the contrasting low-frequency basic state

sea surface temperature (SST) pattern; the MJO and RCC events were associated with anomalously warm and cold low-frequency SSTs prevailing over the western to central Pacific respectively. Differences in the SST anomaly field were absent from the intraseasonal frequency range of 20-60 days. The basic state SST pattern associated with the MJO was characterized by a positive zonal SST gradient from the Indian Ocean (IO) to the western Pacific (WP), which provided a long-standing condition that allowed for sufficient buildup of MSE across the IO to the WP via large-scale low-level convergence over intraseasonal and longer timescales. The results suggested the importance of such basic state SST, with a long-lasting positive zonal SST gradient, for enhancing convection over a longer than intraseasonal timescale to realize a complete MJO lifecycle.

Subsequently, how MJO propagation speed is affected by the background SST was investigated through constructing a tracking method of MJO propagation and comparing the background states that MJO occurred in by their propagation speed. Analysis on the fastest and the slowest 10 MJO events revealed differences in the moist processes that occurred during each of the MJO groups. MSE budget analysis showed that long-lasting deep convection develops across the IO region to the WP region for the slow MJO with preceding build-up of MSE from horizontal advection, and positive feedback to convection from latent and radiative heating terms. On the other hand, for the fast MJO, deep convection developed only for about 10 days, and occurrence of moist processes supporting convection appeared to be confined to the IO. The differences in the accompanied moist processes in slow and fast MJO were associated with different oceanic states that they occurred in; the slower events were associated with a condition of low-frequency SST distribution with a positive zonal gradient from the IO to WP. Low-frequency SST associated with fast MJO were much the same across IO to WP. Significant differences in the SST pattern were not recognized in the intraseasonal timescale of 20-60 days. Furthermore, the extension of the analysis of propagation speed to rest of the events revealed that the relationship between zonal SST gradient and propagation speed was not a tendency restricted to the fastest and the slowest group but is an overall relationship that is

displayed by all of the events. Taking note that the presence of zonal SST gradient in low-frequency range has the potential to enhance large-scale zonal circulation, the component of the zonal wind associated with the background circulation was also analyzed. The analysis showed that there is a tendency for MJO to propagate slower when the background large-scale zonal circulation was stronger, implying that slower MJOs is embedded in enhanced large-scale zonal circulation.

Following this analysis, the reproducibility of such relationship of MJO properties with the background fields in a model simulation was investigated using climate simulation data from an Atmospheric Model Intercomparison Protocol (AMIP) type run with the Nonhydrostatic Icosahedral Atmospheric Model (NICAM). It was found that the simulated MJO events tended to be slower than reality and were biased in the season of their occurrence to late boreal winter. The causes for the systematic slow bias and decrease in the number of boreal summer MJO were related to the difference in monsoonal circulation in the NICAM-AMIP run. Although it appeared that the strength of the background circulation related to MJO propagation speed was being modulated by different reasons than in reality, MJO in NICAM-AMIP still also showed the relationship between its propagation speed and the SST gradient and circulation indices that supported results from real-world MJO.

In summary, this study identified characteristics of the MJO that distinguishes them from other tentative convective activities in the differences in the MSE build-up processes. Such differences were related to the low-frequency SST pattern in which, MJO was associated with a positive zonal SST gradient from IO to the WP. Investigation of how such SST pattern affects the MJO properties showed that MJO propagation speed becomes slower as the zonal SST gradient increases in both observation and NICAM-AMIP simulation. The results of this study indicated the importance of the influence of the low-frequency SST on the MJO and implied that MJO exists as part of the large-scale circulation driven by the low-frequency zonal SST pattern.

Contents

Chapter 1

Introduction

1.1 Characteristics of MJO from observation

The Madden-Julian Oscillation (MJO) is a prominent intraseasonal variability in the tropics, which has been studied extensively since its discovery in 1971 (Madden and Julian, 1971). The phenomenon was first found as a spectral peak in the range of 40-50 days in the co-spectrum of rawinsonde data of sea level pressure, low level (850 hPa) and upper level (150 hPa) zonal winds. From the broad spectral peak at low-frequency range and the phase relationship between the variables, they predicted that the oscillatory signals were from large circulation cells oriented in a zonal plane over the equator. Shortly after, they presented a more detailed picture of the phenomenon as an eastward moving pair of large-scale (O(10,000 km)) circulation cells with enhanced deep convection in the shared region of ascent between the two cells (Madden and Julian, 1972), and this view has been confirmed by others (e.g., Knutson et al., 1987; Hendon and Salby, 1994). Currently, this phenomenon is widely accepted to be an eastward proceeding envelope of convective activity coupled with circulation, typically initiating over the Indian Ocean (IO) and terminating near the dateline (Zhang, 2005).

The spatial structure of the MJO has been well documented. The convective region of MJO is described as an envelope of smaller scale, short-lived convective systems which contributes to the overall eastward movement by developing new convection predominantly eastward of the preceding convection (Nakazawa, 1988). The vertical extent of the cells spans the entire troposphere and takes a baroclinic structure marked with reversal of zonal wind between 600 and 500 hPa level (Madden and Julian, 1971, 1972). The horizontal circulation pattern is characterized by Kelvin response ahead of, and by Rossby response (Matsuno, 1966; Gill, 1980) in the rear of the convective region (Hendon and Salby, 1994). More specifically, MJO convection is preceded by equatorial easterlies and are followed by equatorial westerlies with Rossby gyres on both sides of the equator. At the beginning of the MJO when the convective activity is over the IO, this structure is known to be tilted westward in the vertical and comes into phase before convective activity diminishes over the Pacific (Weickmann and Khalsa, 1990; Hendon and Salby, 1994). The phase relationship between convection and circulation also changes as MJO proceeds eastward. Over the IO circulation signal tends to lag the convective activities, but they come into phase by the time they reach the western Pacific (WP). Furthermore, circulation signals are known to continue their eastward propagation after they decouple with convective activities near the dateline at speeds ranging from approximately 10 ms^{-1} to approximately 40 ms^{-1} (Weickmann and Khalsa, 1990; Milliff and Madden, 1996), which faster than the typical propagation speed of MJO convection of 5 ms^{-1} (Weickmann et al., 1985; Weickmann and Khalsa, 1990).

1.2 Defining the MJO

Because MJO is accompanied by many coherent signals that reflect the presence of its circulation and convection (e.g., outgoing longwave radiation; OLR, wind fields, precipitation, surface pressure), numerous MJO detection methods have been proposed. Adding on to the variety of signals, the episodic nature of the convective events which make up the multi-scale structure of the MJO, and seasonally and geographically varying characteristics of the MJO make it an especially difficult phenomenon to pin down its identity. Reflecting this difficulty, a number of MJO indices have been proposed depending on the choice of physical variables and methods of index construction (e.g., Wang and Rui, 1990; Wheeler and Kiladis, 1999; Wheeler and Hendon, 2004; Kikuchi et al., 2012)). For these reasons, although there is a general agreement on basic features of the MJO, the definitive characteristic of MJO is controversial, and unified definition of this phenomenon is yet to be determined (Straub, 2013; Kiladis et al., 2013).

An often adopted method of MJO definition involves wavenumber-frequency spectrum analysis that extracts eastward propagating signals around 30-60 days period in MJO coherent variables (Hayashi, 1971; Takayabu, 1994; Wheeler and Kiladis, 1999; Yasunaga, 2011). These methods are advantageous in that they can simultaneously detect multiples of theoretically demonstrated equatorial waves (Matsuno, 1966), which are often coexistent with the MJO (Takayabu, 1994; Wheeler and Weickmann, 2001; Masunaga, 2007; Kikuchi, 2014). Another advantage of spectral analysis is that once the range of wavenumber-frequency filtering is set, each mode of tropical convective activity can be defined objectively in both space and time. However, application of spectral analysis implicitly assumes that MJO is an oscillatory wave-like phenomenon which is a questionable prerequisite considering its wide-spread periodicity of 30-100 days (Madden and Julian,

1971; Salby and Hendon, 1994).

Eigen technique is another often used method to construct MJO indices. The Real-time Multivariate MJO index (RMM; Wheeler and Hendon, 2004, WH04) is one of such indices that have been widely applied to identify dates associated with the MJO. The RMM index detects large-scale circulation coupled with convection by applying a combined empirical orthogonal function (CEOF) analysis to a combination of de-seasoned OLR and upper (200 hPa; U200) and lower (850 hPa; U850) level zonal winds data. The time series of the derived first two principal components (RMM1 and RMM2), which interchanges in their relative sign and amplitude, reconstructs the developmental stages of the MJO. The simplicity of implementation, with applicability for real-time use across all seasons, has made it a standard in MJO analysis. A caveat to this method is that high amplitude of the RMM signifies only that the atmosphere assumes an MJO-like pattern in circulation and convection momentarily. Therefore, defining MJO using eigen methods requires careful specifications of criteria for the behavior of principal components in time.

While MJO is often treated as a phenomenon existing in all seasons (Wheeler and Hendon, 2004; Zhang and Dong, 2004; Hendon et al., 2007), MJO characteristics show strong seasonality, and whether the identities of eastward propagating convective activities of a differing season are fundamentally different is still debatable. For example, Bimodal Intraseasonal Oscillation index of Kikuchi et al. (2012) incorporates seasonal variabilities of the MJO and treats intraseasonal variability in the boreal summer as a different mode of atmospheric variability from the MJO. There are also others that claim faster boreal spring events should be associated with convectively-coupled Kelvin waves (Zhang, 2005).

There are still other variants of MJO indices that carefully track convective signal in time and space (e.g., Wang and Rui, 1990; Hendon and Salby, 1994). Although most

of these varying indices have been confirmed to portray similar overall feature of this phenomenon (Straub, 2013; Kiladis et al., 2013), a definition of MJO is often subject to modifications depending on the characteristics of the MJO that is considered essential.

1.3 Eastward propagation of the MJO

The eastward movement of convective activity is one of the most notable characteristics of the MJO. However, the mechanisms for the eastward propagation and how their propagation speed and paths are determined are still not completely understood. Nevertheless, knowledge of statistical properties related to the eastward propagation has accumulated over the years which have contributed to our understanding of the MJO.

Seasonality significantly affects the paths and the ways in which MJO convection moves eastward. In their meticulous tracking of MJO convective activities, Wang and Rui (1990) showed that the path of MJO propagation can be classified into several groups with seasonality. They identified that while MJO in boreal winter months propagates eastward with relatively small meridional movement, boreal summer MJO moves northward after making eastward movement around the Maritime Continents (MC). They also showed that boreal summer MJO was longer and had slower propagation speed than in other seasons. More recently, results consistent with Wang and Rui (1990) have been achieved by Jenkner et al. (2011) who indicated the tendency of boreal spring events to have shorter periodicity. Other researches have shown that variations in propagation speed and frequency are also related to oceanic states within boreal winter MJO (Izumo et al., 2010; Nishimoto and Shiotani, 2013). Further discussions on the relationship between MJO characteristics and oceanic conditions will be presented in the next section.

Propagation of the MJO is also influenced by land-sea distribution. Convective activi-

ties of the MJO often weaken and stagnate over the MC before propagating to the WP, and conditions for successful propagation of convective activities across the MC have become one of the key issues in understanding MJO propagation. The effect of MC hindering MJO convection is known as the "barrier effect" on the MJO, and has been recognized in both observations (Rui and Wang, 1990; Nitta et al., 1992; Hendon and Salby, 1994; Zhang and Ling, 2017) and in simulations (e.g., Inness and Slingo, 2003; Jiang et al., 2015). Preceding researches have suggested that conditions such as the transition from an over-land dominant precipitation regime to an over-sea dominant regime (Zhang and Ling, 2017), and sufficient horizontal advection of moisture and moist static energy (MSE; Miura et al., 2007; Kim et al., 2014; Feng et al., 2015) to be important factors for MJO propagation to the WP. In model simulations, other factors such as the correct representation of low-level winds (Inness et al., 2003) and the choice of cumulus parameterization (Zhu et al., 2017) have been indicated to be important for the successful propagation of the MJO over the MC.

1.4 Air-sea interactions

It has been known that formation of deep convective activities over the ocean is strongly correlated with the sea surface temperature (SST; Graham and Barnett, 1987; Zhang, 1993; Waliser and Graham, 1993). For example, convective activities are enhanced by higher SST with a threshold temperature around 27.5°C, in which deep convection begins to be enhanced (Graham and Barnett, 1987; Zhang, 1993). However, maximum intensification of convection occurs approximately at 29.5°C and convective activity is observed to decrease with an increase of SST from that value (Waliser and Graham, 1993). The explanation of the existence of maximum SST in convection enhancement is offered by

the effect of surface cooling by the enhanced convection, which acts to limit the SST to around 29°C. Therefore, it was suggested that very warm SST can only be achieved under cloudless conditions (Waliser and Graham, 1993). Their results showed that SST conditions not only force convective activities but are expected to be adjusted by atmospheric processes. Considering the significant influence of the sea surface conditions to convective activities, air-sea interaction related to MJO has been studied extensively.

The region in which MJO convection occurs is known as Indo-Pacific warm pool, defined as the area of the IO and the WP within 28°C isotherm (Wyrtki, 1989). This region of high SST is known for its strong seasonal cycle. Location of the Indo-Pacific warm pool shows meridional march following the sun, and its area contracts to its primary and secondary minima in January and August, respectively, and expands to the primary and secondary maxima in April and November, respectively (Kim et al., 2012). The seasonal march of the Indo-Pacific warm pool has been documented to act directly on MJO to regulate its meridional location (Zhang and Dong, 2004). The primary minimum and the secondary maximum is attributed to changes in the WP sector of the warm pool, modulated by the seasonal march of the sun, whereas the secondary minimum and the primary maximum follow the variation of the IO sector, controlled by the Indian monsoons (Kim et al., 2012). The distinct regulation of the two sectors of the warm pool gives rise to a unique background SST distribution in the zonal direction for each season. In relation with the positive zonal gradient formed by the Indo-Pacific warm pool, a result consistent with implications of Lindzen and Nigam (1987) has been achieved by Zhang and Dong (2004) who suggested suggests the importance of background low-level westerlies for the MJO.

Basic schematic of air-sea interaction during MJO has been described in Shinoda et

al. (1998). In the active phase of MJO, reduced radiation and enhanced latent heat flux are observed in the rear of the convective activities due to the high cloud coverage and strong surface westerlies. The opposite condition prevails during the suppressed phase with increased insolation and decreased evaporation. As a response to these atmospheric forcing, a near quadrature pattern of convective signals across the Indo-Pacific warm pool with lagged negative SST response to convection is observed. Typical magnitude of the SST fluctuation has been documented to be around 0.3 K (Shinoda et al., 1998), however, the amplitude of SST anomaly has been reported to exceed 1-2 K for intraseasonal cooling events which could be associated with the MJO (Saji et al., 2006). It has been suggested that SST patterns generated by this air-sea interaction are important for the eastward propagation of the MJO (Flatau et al., 1997; Hirata et al., 2013; DeMott et al., 2014; Zhu et al., 2017). There are also results that indicate the magnitude of the SST change by air-sea interaction during an MJO event to influence the amplitude of the subsequent MJO event (Moum et al., 2016).

Influence of interannual variability on the behavior of MJO has also been investigated (e.g., Izumo et al., 2010; Nishimoto and Shiotani, 2013). Nishimoto and Shiotani (2013) investigated the behavior of eastward propagation of intraseasonal convective activities during boreal winter in relation with the El Niño Southern Oscillation (ENSO), an ocean-atmospheric coupled mode best characterized by the SST anomaly in the eastern Pacific (Trenberth, 1997). They found that slower propagation speed to be associated with La Niña conditions and vice versa. Other works have identified increased MJO activities during boreal spring leading El Niño events in the subsequent autumn-winter season (e.g. Zhang and Gottschalck, 2002; Hendon et al., 2007). On the other hand, Izumo et al. (2010) associated differences in the frequency of the MJO with the Indian Ocean Dipole

(IOD) mode (Saji et al., 1999). The IOD is recognized as a dipole mode of SST anomaly in the IO in which the positive phase is associated with high SST in the western Indian Ocean (Saji et al., 1999). High and low-frequency MJO, with respective frequency of 35-50 days and 55-100 days, are distinguished to occur under opposite IOD mode; high-frequency MJOs in positive IOD and low-frequency MJOs in negative IOD (Izumo et al., 2010). There are also other studies that indicated enhanced and subdued MJO activities with negative and positive IOD, respectively (Wilson et al., 2013). In their work, weakening of the MJO during positive IOD was related to the inhibition of low-level convergence from the SST gradient anomalies from IOD and associated low-level wind anomalies (Inness et al., 2003). Consistent results regarding MJO-IOD relationship have also been achieved by Benedict et al. (2015) for October condition in model experiments. However, there are other results that assert the influence of interannual variability on MJO to be limited (Hendon et al., 1999; Slingo et al., 1999).

1.5 Moisture mode theory

A school of thought, referred to as moisture mode theory, which attempts to theoretically explain MJO by prognostic moisture equation (e.g. Neelin and Held, 1987; Sobel and Maloney, 2012, 2013; Adames and Kim, 2016) has gained popularity in the recent years. Based on the weak temperature gradient approximation (WTG; Charney, 1963; Sobel et al., 2001), which states that horizontal gradient of temperature is bound to be small in the tropics due to the smallness of the Coriolis parameter, modulation of moisture anomaly becomes essential to destabilization and enhancement of convective activities in the tropics. From the WTG, the moisture mode theory establishes a concept that MJO is not analogous to any of the dynamical modes in the dry atmosphere, and that moist

process is of fundamental importance for its growth and propagation. Other processes including ocean coupling are thought to be subordinate. In the moisture mode framework, the growth of convective activity is governed by processes such as surface fluxes and cloud-radiative feedback that modulate moisture anomaly (Sobel and Maloney, 2012, 2013). In their original models based on the moisture mode, the one-dimensional equation for column integrated water vapor in the zonal direction is the only prognostic equation describing the mechanism of the MJO. All other fields are determined diagnostically using empirical closure assumptions. The moisture mode models with certain conditions were capable of reproducing eastward propagating moisture modes at the largest horizontal scales. However, their model relies on questionable requirements on the background moisture advection for eastward propagation to occur. Moreover, the eastward propagation speed of the eastward propagating mode was small, and the eastward propagation of the MJO is primarily dependent on zonal advection by background westerlies (Sobel and Maloney, 2013). Recently, work by Sobel and Maloney (2012, 2013) was extended to three dimensional moisture mode model (Adames and Kim, 2016). The model by Adames and Kim (2016) describes the MJO as a dispersive convectively coupled moisture wave with westward group velocity and derives a dispersion relation in good agreement with wavenumber-frequency range of the MJO. Notwithstanding the consistency of the dispersion curve to MJO signals, the model depends on some ambiguous scaling and closure assumptions and requires further investigation for a comprehensive description of the MJO. Although the moisture mode theories have not succeeded in explaining MJO mechanisms completely, investigation of their model behavior, and comparison of the observational data and simulated results with their framework have contributed to the better understanding of moist processes in the tropics (Sobel et al., 2014; Hannah and Maloney,

2014).

1.6 MJO in model simulations

MJO is infamous for its difficulty in reproducing them in model simulations (e.g., Kim et al., 2011; Jiang et al., 2015), and it has only been in the past decade that some models have been able to simulate MJO with adequate correspondence with the observed MJO. One of the first successful realistic simulations of the MJO was achieved (Miura et al., 2007) by using Nonhydrostatic Icosahedral Atmospheric Model (NICAM; Tomita and Satoh, 2004; Satoh et al., 2008), a model which eliminated convective parameterization by computing cloud microphysics explicitly. Model simulation studies using NICAM have since contributed to MJO studies through hindcasts (e.g., Miyakawa et al., 2014; Miura et al., 2016) and sensitivity studies (e.g., Miura et al., 2009, 2016), indicating the potential timescale of predictability of the MJO to be near 4 weeks (Miyakawa et al., 2014) and influence of SST zonal gradient on MJO propagation (Miura et al., 2009; Yoshizaki et al., 2012; Miura et al., 2016). The behavior of MJO-like convective activities in NICAM have also been investigated (e.g., Yoshizaki et al., 2012; Takasuka et al., 2015)) in idealized aquaplanet settings (Tomita et al., 2005). Climatological properties of the MJO within NICAM have been investigated (Kikuchi et al., 2017) from a 30-year climatological run (Kodama et al., 2015) on NICAM following the Atmospheric Model Intercomparison Project(AMIP; Gates, 1992) Protocol.

Although conventional general circulation models (GCMs), that employ cumulus parameterizations have also demonstrated ability to reproduce MJO (e.g., Bechtold et al., 2008), successfully simulating MJO in GCMs remains to be a challenging problem (Jiang et al., 2015). Reproducing the eastward propagation of MJO has been documented to

rely on many factors such as the choice of cumulus parameterization scheme (Maloney and Hartmann, 2001; Chikira and Sugiyama, 2013; Feng et al., 2015), tuning of detrainment (Hannah and Maloney, 2014), coupling with the ocean (Inness and Slingo, 2003; Klingaman and Woolnough, 2014; DeMott et al., 2014), and initial ocean-atmospheric conditions (Kim et al., 2016). However, even in models in which eastward propagation of convective activity is simulated, it is difficult to distinguish whether the model has reproduced eastward propagation of the MJO for dynamically realistic reasons (Hannah and Maloney, 2014). Therefore, identifying essential mechanisms and factors for MJO development and propagation is still a challenging task to undertake using the model alone.

There are also efforts to bridge the gap between MJO simulation in GCMs and cloud resolving models by the use of super-parameterization (Grabowski, 2001; Benedict and Randall, 2009), which embeds two-dimensional cloud resolving model within a grid of GCM to compute statistical properties of the grid (Grabowski, 2001). A number of studies indicate improved MJO representation in superparameterized models to its counterpart GCMs (e.g., Klingaman and Woolnough, 2014; Hannah et al., 2015, and references therein). However, why the performance of the superparameterized models excels the conventional GCMs is still unclear (Hannah et al., 2015), and the causes for the differences need to be investigated further.

1.7 Motivation and overview

Despite being the most prominent intraseasonal variability in the tropics, essential factors for the realization of the MJO and what modulates their properties are still controversial. In consideration of the difficulties that MJO posed in explaining it as a unique dynamical mode of the atmosphere, this research seeks for an explanation for the exis-

tence of the MJO from an alternative point of view, that MJO might be explained as a forced response from the large-scale environment. This is based on a hypothesis that for an MJO-like large-scale atmospheric circulation to develop and to persist on an intraseasonal timescale, a background state longer than the intraseasonal timescale should provide long-standing conditions that support the development of MJO convection. Foundations for this hypothesis were investigated in this study, and the overview is given below.

In chapter 2, an objective MJO detection method was constructed applying the WH04 RMM method. Here MJO-like atmospheric patterns were classified as MJO and regionally confined convective (RCC) events so that they can be compared to reveal essential properties of the MJO that distinguish them from other tentative convective events. [1,2] A tracking method of MJO convection was also developed to analyze the propagation speed of the MJO.

In chapter 3, an environment favorable for the development of the MJO was investigated from a comparison of MJO and RCC events. Moist processes related to the MJO and RCC were analyzed from MSE budget analysis, and the differences that were observed were related to the low-frequency variability of the SST.

In chapter 4, differences in the MJO properties arising from those in their propagation speed were analyzed. MJO events were categorized into slow events and fast events to

[1]Part of chapter 2 regarding the detection method of MJO and RCC, and chapter 3 is published as Suematsu, T., and H. Miura, 2018: "Zonal SST difference as a potential environmental factor supporting the longevity of the Madden-Julian Oscillation". J. Climate. doi:10.1175/JCLI-D-17-0822.1

reveal factors that modulate their propagation speed. The analysis was later extended to all detected MJO events to find a general relationship of the MJO propagation speed and the environment.

In chapter 5, the analysis conducted on the reanalysis data is applied to data from NICAM-AMIP simulation. The reproducibility of relationship of MJO properties with the background fields that were found in the preceding chapters in model simulation was investigated. Differences and similarities between the simulated MJO and the real world, and their causes were discussed.

Chapter 6 provides summary, discussions, and general conclusions on the obtained results. The outlook for future work will also be presented.

Chapter 2

Data and method

2.1 Data

[1] This study employed the following standard datasets for calculating the RMM index: daily averages of the interpolated OLR (Liebmann and Smith, 1996) from the National Oceanic and Atmospheric Administration (NOAA), and daily averages of U850 and U200 from the National Centers for Environmental Prediction-National Center for Atmospheric Research (NCEP-NCAR) Reanalysis 1 (Kalnay et al., 1996). The analysis spanned a period from 1 January 1979 to 31 December 2012 with a horizontal resolution of $2.5° \times 2.5°$. These choices are made to facilitate comparison with the results of previous studies, and to keep within the range of the final product of WH04 RMM provided by Australian Bureau of Meteorology (2018) which ends on 31 December 2013. However, it is confirmed that extending the analysis period to 31 December 2016 does not change the general conclusion of this study. We also used the daily values of the NCEP-NCAR Reanalysis 1 data for the variables required to calculate the MSE budget terms.

[1]This section is published as Suematsu, T., and H. Miura, 2018: "Zonal SST difference as a potential environmental factor supporting the longevity of the Madden-Julian Oscillation". J. Climate. doi:10.1175/JCLI-D-17-0822.1

The NOAA Optimum Interpolated SST V2 (OISST; Reynolds et al., 2002) was analyzed from 1 January 1982 to 31 December 2012 to investigate the background SST state favorable for MJO development. The resolution of the OISST ($0.25^\circ \times 0.25^\circ$) was reduced to the resolution of the other NCEP-NCAR data ($2.5^\circ \times 2.5^\circ$), by using area averaging. This reduction was validated by analyzing the spatial scale at which SST became coherent with convective activity in the tropics. This was achieved by investigating the resolution at which the SST and the total column water (TCW), which is closely related to convective activity in the tropics (Bretherton et al., 2004), becomes well correlated. For consistency between the TCW and SST within this analysis, European Reanalysis Interim data (ERA-I; Dee et al., 2011) provided in 11 different resolutions between $0.125^\circ \times 0.125^\circ$ and $3.0^\circ \times 3.0^\circ$ for both TCW and SST was used. The correlation of SST and TCW was calculated between 30° S and 30° N, at resolutions of $0.25^\circ \times 0.25^\circ$, $1.0^\circ \times 1.0^\circ$, $2.5^\circ \times 2.5^\circ$ using the original ERA-I data from 1 January 1982 to 31 December 2015 (Fig. 2.1). Correlations at lower resolutions at $5.0^\circ \times 5.0^\circ$ and $10.0^\circ \times 10.0^\circ$ were also calculated by area averaging the $2.5^\circ \times 2.5^\circ$ data to those resolutions. Figure 2.1 shows that the correlation between SST and TCW was low for higher resolution data. However, the correlation increased above 0.6 when the resolution was reduced below $2.5^\circ \times 2.5^\circ$ resolution. Therefore, it was determined that reduction of the resolution of SST data to $2.5^\circ \times 2.5^\circ$ was reasonable for this study, which is intended to examine the effect of SST on convective activities over the tropics.

It was noted that the September 1994 OLR data had unrealistically high values with respect to the satellite switching between 16 September and 17 September. Consequently, data of 1 May 1994 to 31 January 1995 were omitted to eliminate data contaminated from satellite switching by the time-filtering.

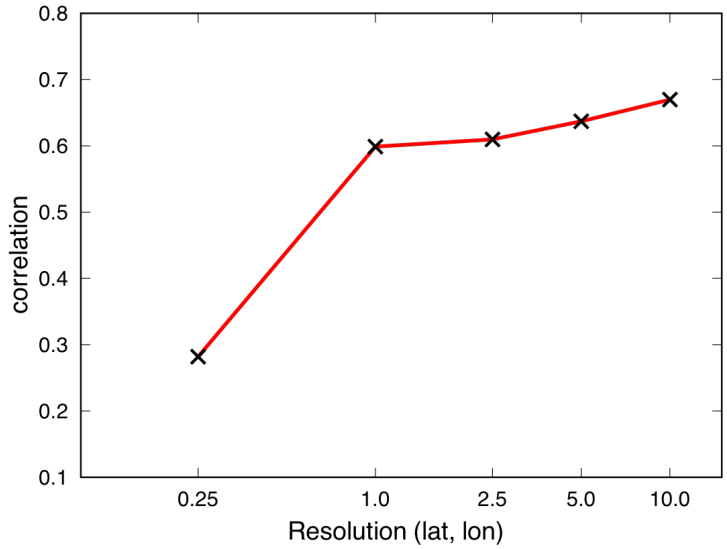

Figure 2.1: Resolution dependency of the correlation between SST and TCW from the ERA-I over the tropics (30°S-30°N)

2.2 Detecting MJO and RCC

[2] This study applied the RMM method of WH04 to detect MJO events. However, the purpose of this study is not a real-time evaluation of the MJO; hence, we simplified the de-seasoning process of the original WH04 to 20-120 day Lanczos band-pass filtering (Duchon, 1979). The filter employed 241 symmetric weights, and 120 days at both ends of the data were truncated. A relatively wide window for the band-pass filter was used to include signals on a near-seasonal time scale in consideration of MJO events that appeared to be driven by the seasonal cycle (Miura et al., 2016). With the exception of utilizing this band-pass filtered data, the RMM calculation followed that of the original WH04 RMM. Although the resulting RMM series had a smoother trajectory than the original WH04 RMM series (Fig.2.2), the overall features were consistent with those of WH04

Here, to capture the MJO as an entity of eastward propagating convective activity on

[2]This section is published as Suematsu, T., and H. Miura, 2018: "Zonal SST difference as a potential environmental factor supporting the longevity of the Madden-Julian Oscillation". J. Climate. doi:10.1175/JCLI-D-17-0822.1

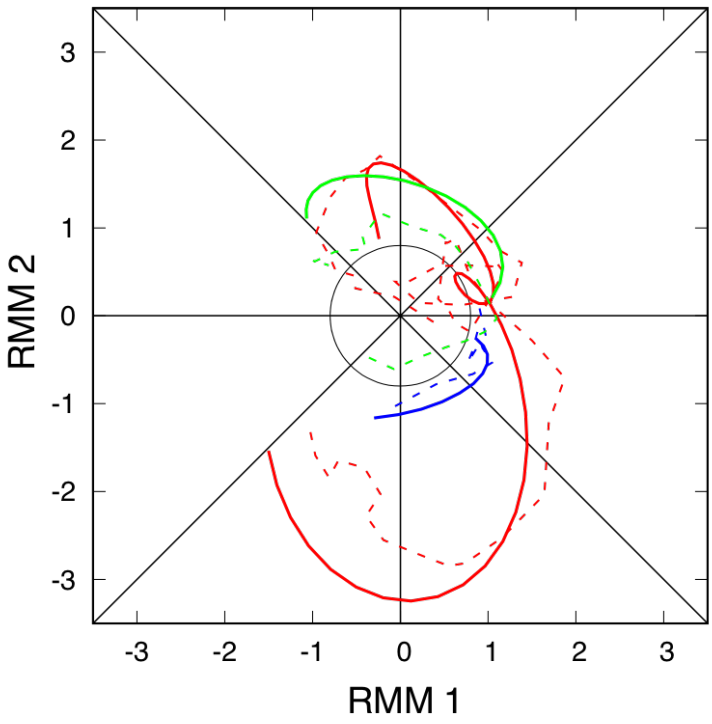

Figure 2.2: Examples of MJO (red), IO-RCC (blue), and WP-RCC (green) RMM trajectories. Solid lines indicate RMM trajectories calculated by using the 20-120 day filter, and dotted lines indicate RMM trajectories of the original WH04 RMM trajectories provided by Australian Bureau of Meteorology. The trajectories shown are from 13 January 2002 to 5 March 2002 for the MJO, 7 January 1982 to 17 January 1982 for the IO-RCC, and 17 November 1989 to 5 December 1989 for the WP-RCC event. The inner circle indicates RMM amplitude of $A_c = 0.8$.

an intraseasonal timescale, identification of MJO events using the RMM requires consideration of the continuity of the trajectory of the RMM projection in the RMM phase space. Intermittent occurrences of days with high RMM amplitudes need to be distinguished from the MJO by defining the MJO as a time sequence with an RMM projection trajectory that signifies continuous eastward propagation of convective activity from the IO to the WP. Therefore, MJO was defined by specifying a set of criteria to be met by the RMM trajectory, the physical implications of which are consistent with the general characteristics of the MJO. The MJO criteria, followed by their concise physical implications in parentheses, are as follows: 1) It proceeds from at least phase 2 to phase 7

(large-scale circulation propagates through the IO to the WP); 2) it does not skip more than one phase (continuous propagation in real space); 3) it does not recede more than one phase (disqualification of major westward propagating events); 4) the average RMM amplitude exceeds the critical value A_c, and consecutive days with an amplitude below A_c are fewer than 15 days (maintenance of typical MJO structure); and 5) the tracking is completed in 20-90 days (completion of an event within an intraseasonal time scale). The value of A_c was subjectively set at 0.8 because a sufficiently strong signal of MJO-like atmospheric pattern appeared to be present when the RMM amplitude was at least 0.8 (Fig. 2.2). For example, the RMM amplitude dropped below A_c for four days during the MJO event shown in Fig. 2.3, which corresponds to the MJO trajectory in Fig. 2.2. However, strong eastward-proceeding convective activity was present even when the RMM amplitude was small. The critical value was set at 0.8 rather than a higher value to maximize the number of MJO events. Moreover, it was confirmed that the general conclusions of this study were insensitive to A_c values between 0.8 and 1.0.

The criteria were relaxed from a strict anticlockwise procession on the RMM phase space to allow for some skipping and receding of RMM phases and for a temporal drop in RMM amplitude. These criteria were implemented in consideration of the existence of small-scale disturbances within the MJO that may cause temporary jumps, reversals, and amplitude drops of the RMM (Fig. 2.2). Relaxation of the criteria has the effect of making the MJO detection insensitive to unrealistic phase flips. We note that different measures for the same purpose have been implemented in preceding researches (e.g., Matthews, 2008).

Following the criteria, MJO events were detected by first identifying those days projected on phase 2 and then tracking back to phase 1 and forward up to phase 8. Backward

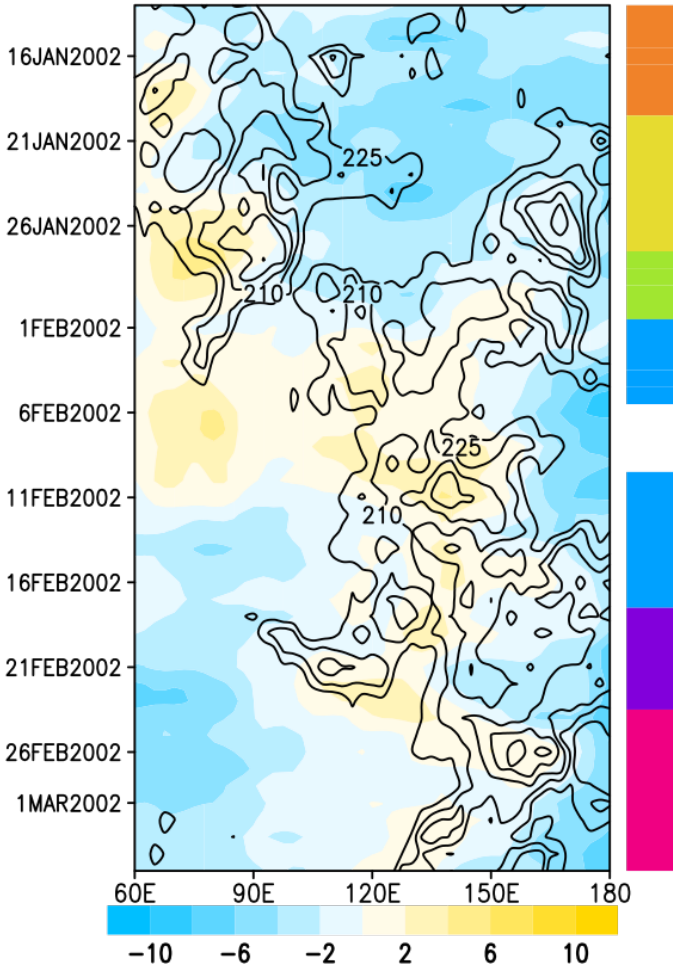

Figure 2.3: 15°S-15°N averaged U850 (color; ms^{-1}) and OLR (contour; Wm^{-2}) time-longitude Hovmöller during an MJO event from 13 January 2002 to 5 March 2002. The color bar on the right indicates the daily RMM phase; orange, phase 2; yellow, phase 3; light-green, phase 4; blue, phase 5; purple, phase 6; and magenta, phase 7. Periods without color indicate days when the RMM amplitude was lower than A_c.

tracking terminated when the RMM amplitude fell below A_c or when a phase change occurred. Forward tracking was terminated when the RMM amplitude fell below A_c any time after the first day of phase 7. Tracking was also terminated when a phase change occurred after the first day of phase 8. We defined the initiation and termination of the active phase of the MJO as the first and the last day of phase 2 and phase 7, respectively. Because the attribution of an RMM phase is not legitimate when the amplitude is small, phase retreat or procession is considered only when the RMM amplitude exceeds

A_c. In this way, 112 MJO events were detected during 1982-2012 with the removal of two events from May 1994 to January 1995, the period in which the Lanczos-filtered data were contaminated by data from September 1994.

Days with an RMM amplitude greater than A_c were further categorized into two types of regionally confined convective events (RCC); Indian Ocean (IO)-RCC and Western Pacific (WP)-RCC, depending on the location of their occurrence. We defined IO-RCC and WP-RCC as events of RMM amplification above A_c, that were not part of MJO events and were restricted to phases within 2-4 and phases 5-7, respectively (Fig. 2.2). Initiation of IO-RCC and WP-RCC was defined by the first day of the RMM amplification within the respective phase range; an event was terminated when the RMM amplitude dropped below A_c at any time after initiation. Any amplification of RMM not included in the above categories (e.g., RMM amplification that spans phases 2-5) was not considered in this research. In this way, we distinguished temporary events of RMM amplification from conventional MJO events, which are usually complemented by amplification of RMM phases in RMM phase ranges of both IO-RCC and WP-RCC. In this study 51 IO-RCC events and 55 WP-RCC events were identified.

The method described in this section is not definitive for identifying MJO events or RCC. However, this method is sufficient for the purpose for this study in designating an adequate number of convective events that demonstrate the conventional properties of MJO as MJO events and those of other regionally confined and short-lived convective events as RCC events. The results obtained enable their properties to be analyzed and compared statistically. We also note that although RMM is predominantly determined by large-scale circulation (Straub, 2013), this method captures large-scale convective activity events in terms of signal strength and spatial scale as adequately as other MJO detecting

methods that use only OLR values (e.g., Matthews, 2008; Hirata et al., 2013).

2.3 Tracking MJO convective activity

Eastward movement of each detected MJO event was tracked daily by the zonal location of the minimum value in the 15°S-15°N meridionally averaged OLR (Fig. 2.4). The daily tracking was done in zonal range depending on the RMM phase of the day of the tracking. The tracking was also restricted to OLR value less than 210 Wm^{-2} to ensure that there is a signal of convective activity where minimum OLR was located. The zonal ranges of tracking for each RMM phase are as follows: For phases 1-3, the tracking was done in the range of 50°E to 120 °E; for phase 4 tracking was done in the range of 50 to 150°E; for phase 5 tracking was done in the range of 120°E to 140° W; for phases 6-8 the tracking was done in the range of 150°E to 140°W. During days when the RMM amplitude dropped below A_c, tracking was done in the range of 50°E to 140°W since the designation of an RMM phase is considered to be invalid when RMM amplitude is small. There is an overlap of tracking range during phases 4 and 5 to smoothly track the passage of convective activities over the MC where convection is often blocked, and where convective activities are present on both eastern and western sides of the MC. After tracking the longitude of minimum OLR, the eastward propagation speed of MJO was determined by calculating the regression coefficient between time and longitude of the tracked minimum OLR from the first day of phase 2 to the last day of phase 7 of each MJO event. The calculated regression coefficient was determined to represent the average propagation speed of the MJO if it passed the student's t-test at a confidence level of 95 %. As the result of the statistical test, seven events were removed from the analysis regarding the propagation speed.

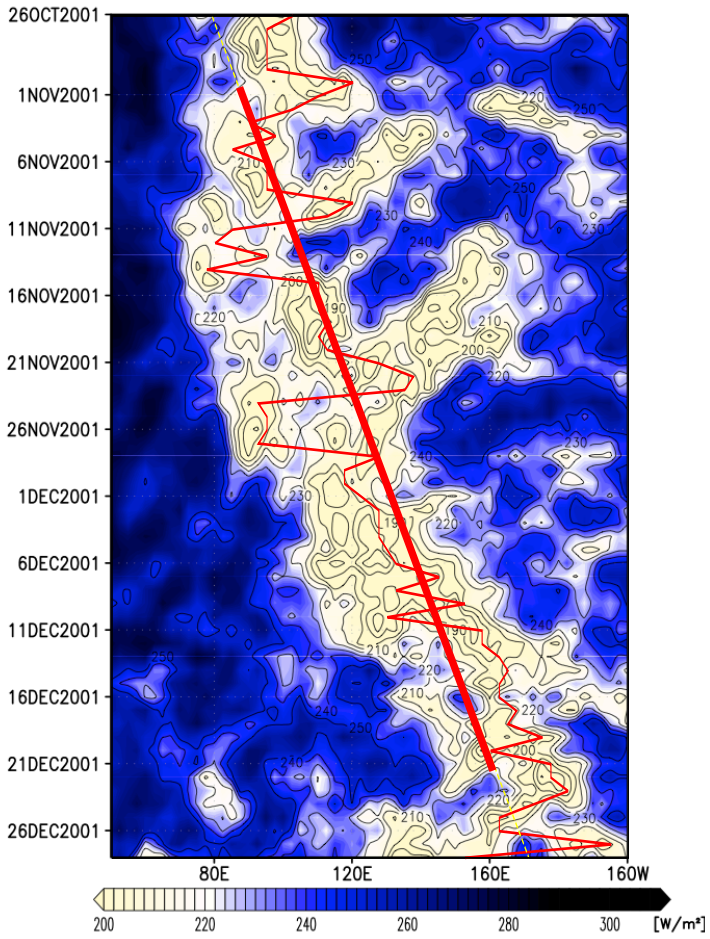

Figure 2.4: An example of minimum OLR tracking (thin red line) during an MJO event and its regression from the first day of phase 2 to the last day of phase 7 (thick straight red line). Color shows 15°S-15°N averaged OLR (Wm^{-2}).

2.4 Checking consistency between propagation speed and angular speed

Consistency between the propagation speed calculated from the tracking of OLR minimum and the behavior of MJO on the RMM phase space was checked. This was done by checking for a linear relationship between the propagation speed calculated in real space and the angular velocity on the RMM phase space (Fig. 2.5). The average angular velocity of each MJO event was calculated by dividing the angle between the first day of phase 2 and the last day of phase 7 on the RMM phase space by the number of days in that

period. Since each phase of the RMM phase space assumes convective activity over the different location from western to central IO to western to central Pacific, angular velocity on the RMM phase space should correspond to and show a linear relationship between the propagation speed calculated by OLR tracking in real space. Therefore to confirm consistency between angular velocity and propagation speed, events that show a linear relationship between angular velocity and propagation speed was selected. The selection was done by calculating the regression line of the angular velocity and propagation speed and selecting the events that were within 2 standard deviations of the residual from the regression line. Three events were removed in this process, and the propagation speed of 102 MJO events was estimated.

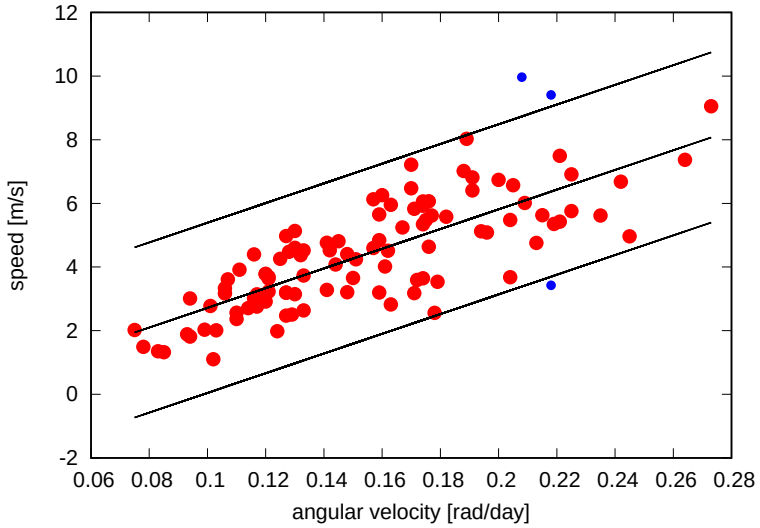

Figure 2.5: Propagation speed-angular velocity plot of detected MJO events. The black lines indicate the regression line of the plot and 2 standard deviations of the residual from the regression line. The red dots are the events included, and the blue dots are the events removed from the analysis.

Chapter 3

Background SST and moist processes for the MJO realization

[1] In contrast to the extensive work that has already been undertaken on the MJO based on the RMM (c.f., Zhang 2013, and references therein), there has been limited research regarding what distinguishes the MJO from discontinuous events of RMM amplification. Hirata et al. (2013) identified convective events that are regionally confined, either over the IO or around the MC, and suggested that the intensity of convective suppression was an important factor in determining the behavior of subsequent active convection. Kim et al. (2014) also investigated the differences between propagating and non-propagating MJO, and their results indicated the importance of the development of a strong dry anomaly prior to the propagating MJO. Moreover, precursor signals for MJO initiation that are absent from large-scale convective events with a low RMM amplitude have been documented by Ling et al. (2013), and factors associated with the termination of MJO events at different RMM phases have been investigated by Stachnik et al. (2015).

[1]This chapter is published as Suematsu, T., and H. Miura, 2018: "Zonal SST difference as a potential environmental factor supporting the longevity of the Madden-Julian Oscillation". J. Climate. doi:10.1175/JCLI-D-17-0822.1

However, it is uncertain as to whether there is a background state longer than the intraseasonal timescale that provides long-standing conditions supporting MJO development. This consideration is supported by theoretical work which shows that a slowly eastward propagating pattern like the MJO can be reproduced through the interaction of wave activities with planetary-scale moisture anomalies (Majda and Stechmann, 2009). I hypothesize that such a basic state condition should exist to allow an MJO-like large-scale atmospheric circulation to develop and to persist on an intraseasonal timescale. This study investigates this hypothesis by focusing on differences in the basic state SST, which provides a bottom boundary condition for much of the convective region of MJO events, and reveals essential environmental factors for the MJO development.

3.1 Characterizing MJO and RCC convection

The circulation and convection patterns of MJO and RCC were compared by using composites of anomaly fields for OLR and U850. Anomalies were calculated by subtracting the daily climatology of the period of 1 January 1982 to 31 December 2011. Differences in circulation and convection between the MJO and the RCCs are apparent in the composite time-longitude Hovmöller diagrams of the meridionally averaged (15°S-15°N) anomalies of OLR and U850 centered at the initiation of the active phase of the MJO which is the first day of phase 2; IO-RCC; and WP-RCC (Fig. 3.1). In the MJO composite, strong signals of both negative OLR and positive U850 anomalies propagated from approximately 60°E to approximately 180°W over 30 days. However, these signals were short-lived, weaker, and stagnant for the RCCs. Signals of convective activity with durations of 10-15 days were present only at approximately 60°E-100°E for the IO-RCC and approximately 120°E-180°E for the WP-RCC. It is also noted that although

the applied composite ignored the differences in the propagation speed of MJO events, it captured the eastward propagation of the MJO and clarified the differences between MJO and RCCs. These results fit the objective of the present analysis and differences in the characteristics of the MJO arising from the differences in the propagation speed will be discussed in the next chapter.

In terms of the signal for convective suppression, interesting similarities were noticed between the MJO and RCCs (Fig. 3.1). For example, the convective activities of both the MJO and IO-RCC were preceded by a signal of anomalously positive OLR that slowly propagated eastward from approximately 60°E to 180°E over 30 days and ended with displacement or diminishment of convective activity over the IO (Fig. 3.1 a, b). Furthermore, the amplitude of the positive OLR anomaly found in the IO-RCC is comparable to that of the MJO over the IO and WP regions. On the contrary, the WP-RCC convective activity over the WP did not appear to be preceded by significant convective suppression over the same region. However, the WP-RCC convective activities were accompanied by a strong signal of positive OLR over the IO region that continued to propagate eastward to the WP well after the convective activity had diminished (Fig. 3.1 c). Furthermore, the magnitude of convective suppression in the WP-RCC was significantly stronger than the signal of convective activity, whereas these signals were comparable for the MJO. This indicates that convective suppression in the IO contributes more to the RMM projection than to convective enhancement in the WP. Therefore, it appears that the onset of an MJO event and an RCC event is difficult to distinguish solely from the projection of atmospheric circulation and convection patterns to the RMM. Moreover, the preceding suppression detected by this composite analysis is not a sufficient condition for the eastward propagation of convection nor is it necessary for initiating a burst of a large-scale

convective event.

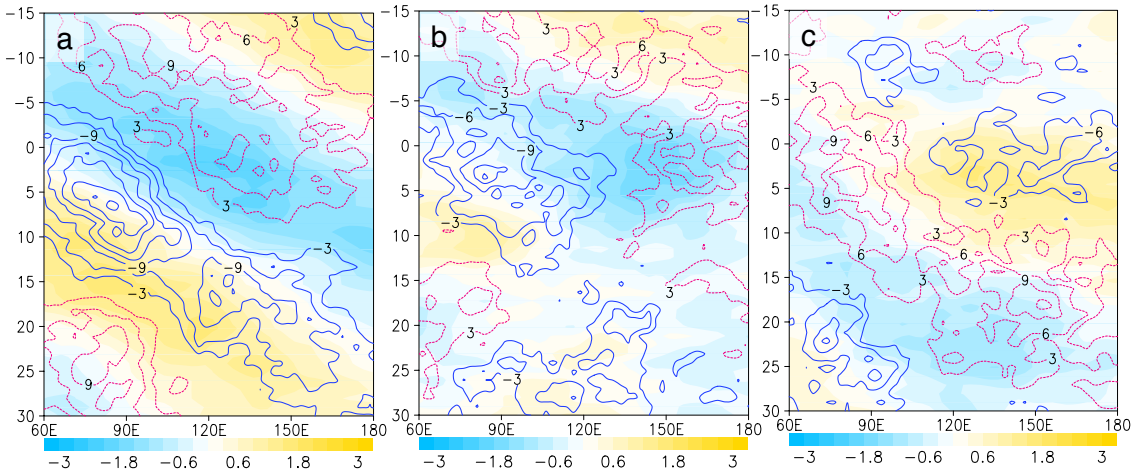

Figure 3.1: Composite Hovmöller of 15°S-15°N averaged anomalies of OLR (contours; Wm^{-2}) and U850 (color; ms^{-1}) for the (a) MJO, (b) IO-RCC, and (c) WP-RCC. Negative OLR anomalies are indicated by blue solid lines and positive OLR anomalies are indicated by magenta dotted lines. Contours are at 3 Wm^{-2} intervals

Differences in the spatial patterns of convection between the MJO and RCCs were compared by using OLR anomaly composites (Figs. 3.2 and 3.3). We compared the OLR anomaly composites of the IO-RCC and WP-RCC on day 0 with the MJO composite at day 0 and at day 15, respectively. The composite dates of the MJO were chosen to ensure that the location of the negative OLR signal approximately matched that of the RCC types at its initiation on the composite Hovmöller diagram. Comparison of the MJO and IO-RCC initiation OLR anomalies shows that although both indicate large-scale convection over the IO region, the IO-RCC convective activity was weaker, and the center was shifted eastward. This could have been caused by the wider range of RMM phases that occurs with IO-RCC initiation. Correspondingly, the suppression signal also shifted eastward for the IO-RCC as compared with the MJO. On the contrary, the WP-RCC initiation was characterized by strong suppression over the IO and multiple smaller patches of convective activity over the WP. It is apparent that the WP-RCC lacks the robust

and widespread negative OLR signal across the eastern edge of the MC to the WP found in the MJO. This suggests that the WP-RCC is characterized by the prevailing conditions of convective inhibition over the IO rather than by convection enhancement over the WP. It is understandable that projection of the RMM to such an atmospheric state is high in phases 5-7 owing to the high sensitivity of RMM to signals over the IO. The sensitivity of RMM to convective signals over the IO arises from the spatial structure of the EOFs of RMM, in which the highest normalized magnitude for OLR occurs around 90°E in EOF2 (WH04). On the basis of these results, further analysis was restricted to the IO-RCC and MJO because it was considered that comparing the WP-RCC and MJO was not expedient in investigating the properties that distinguish the MJO from other large-scale convective events.

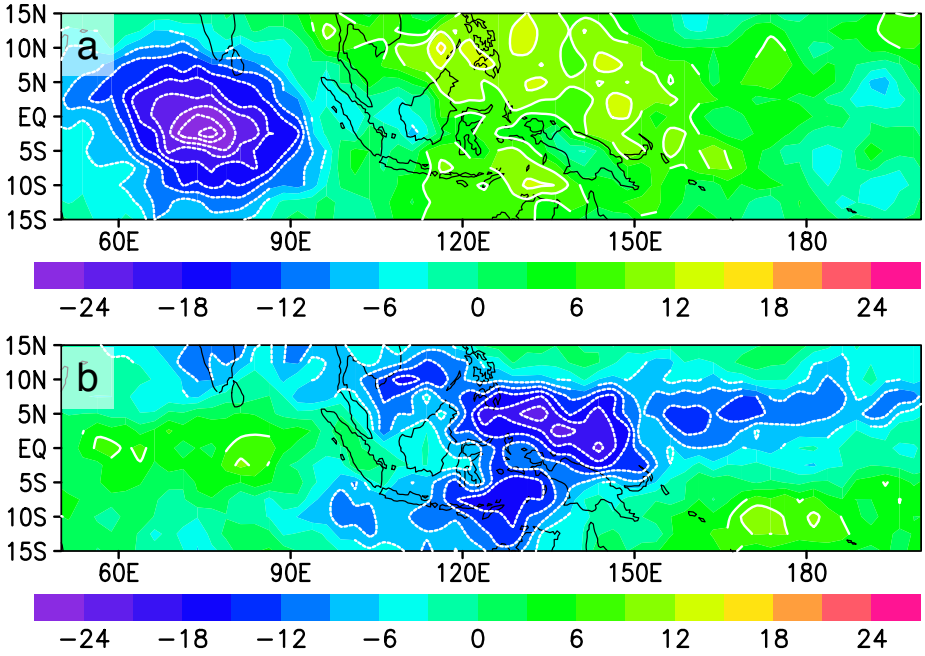

Figure 3.2: Composite of OLR anomalies (Wm^{-2}) of the MJO at day 0 (a) and at day 15 (b). White contours indicate where the signal is statistically significant at 90%.

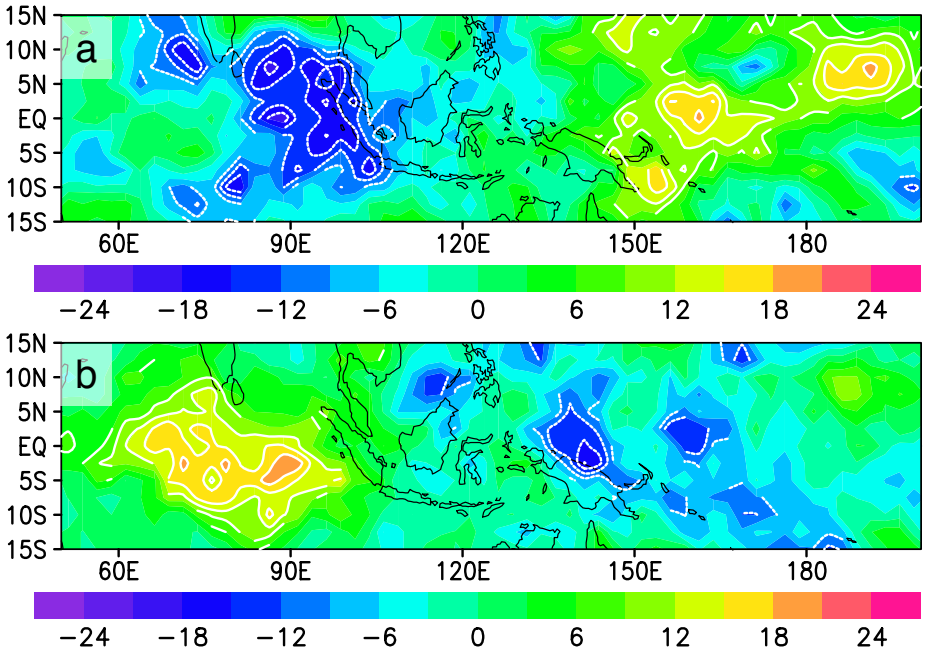

Figure 3.3: Composite of OLR anomalies (Wm^{-2}) for IO-RCC (a) and WP-RCC (b) on day 0. White contours indicate where the signal is statistically significant at 90%.

3.2 Moist processes during MJO and IO-RCC

To compare the characteristics of the moisture budget that drives the circulation of MJO and IO-RCC convection, column integrated MSE budget analysis (e.g., Sobel et al., 2014) was conducted. The column integrated MSE budget equation can be written as

$$< \frac{\partial h}{\partial t} >= - < \boldsymbol{v} \cdot \nabla h > - < \omega \frac{\partial h}{\partial p} > + < \mathrm{LW} > + < \mathrm{SW} > + \mathrm{LH} + \mathrm{SH} \qquad (3.1)$$

where h is the MSE, v is the velocity, LH and SH are the surface latent and sensible heat fluxes, respectively, and LW and SW are the longwave and shortwave heating rates, respectively, and the brackets

$$< X >= \frac{1}{g} \int_{p_{\mathrm{top}}}^{p_{\mathrm{surface}}} X dp \qquad (3.2)$$

denote column integration.

It is noted here that the MSE budget terms are calculated from the reanalysis data which are assimilation products that ingest observational data. The certainty of the diagnostic variables of the reanalysis products is limited by the uncertainties of the parameterizations employed in the model. Therefore, diagnostic variables involved with the hydrological cycle (e.g., evaporation) need to be used with special caution as they are products from parameterizations of highly uncertain processes. It follows that the interpretation of the MSE budget analysis requires careful consideration of its uncertainties. For example, it is well known that MSE budget analysis using reanalysis data includes substantial residual term (Kiranmayi and Maloney, 2011). The magnitude and fluctuation of each MSE budget term should be interpreted qualitatively, and independently from each other rather than in relation with the other terms.

To analyze the MSE budget terms across the regions where MJO convection is active, the equatorial region (5°S-5°N) from 50°E to 160°W was divided into three segments of 50° longitude to represent the IO (50°E-100°E), MC (100°E-150°E) and WP (150°E-160°W) from west to east. The time evolutions of the 11-day smoothed anomaly of the MSE budget terms of each regional segment between the MJO and IO-RCC are shown in Figs. 3.4 and 3.5. Composites of the time evolution were centered at the initial day of the active period of the MJO and IO-RCC as in the previous analysis.

The MSE budget analysis shows that the convective activities of the MJO are organized into a system that interacts with the large-scale environment to induce cooperative energy fluxes and advective processes for convective activity. The occurrence of deep convection during MJO is indicated by the development of anomalously negative vertical advection. At its peak, vertical advection becomes the dominant term in the MSE budget equation.

Large increases in radiative heating that coincide with decreases in MSE vertical advection also imply the development of clouds at high altitudes. The minimum of the vertical advection term in each region is preceded by high horizontal advection of MSE, which implies that during MJO, horizontal advection builds up the MSE eastward of the convective center. This is confirmed by the temporal evolution of the column integrated MSE anomaly (Fig. 3.6 b).

Eastward movement of the column integrated MSE anomaly is demonstrated by its later peak occurrence over the eastward regions, which was approximately day 5 for the IO, day 10 for the MC and day 20 for the WP. It is also noted that horizontal MSE advection over the MC region was especially high where the MJO is frequently blocked, which could have contributed to the successful eastward passage of MJO convection over the MC to the WP. These results are consistent with those in previous studies that suggest the importance of horizontal MSE advection for the eastward propagation of the MJO (Sobel et al., 2014; Kim et al., 2014). The rise in latent heat flux lagged the convective signal by approximately five days over the IO, but was nearly in phase by the time the MJO was over the WP. This result is consistent with Hendon and Salby (1994) who showed that low-level westerlies which lagged convective activity over the IO came into phase as the MJO proceeded to the WP.

Fluctuation of the MSE budget terms associated with activities of deep convection, such as the vertical advection and net radiation terms, was significantly weaker for the IO-RCC and appeared only over the IO and MC (Fig. 3.5). Over the IO, the peak vertical advection term was approximately half, and the peak radiative heating term was approximately one-third of the peak values during the MJO. By the time convection shifted eastward to the MC, the magnitude of these signals was even weaker. Over the WP, the signs of these

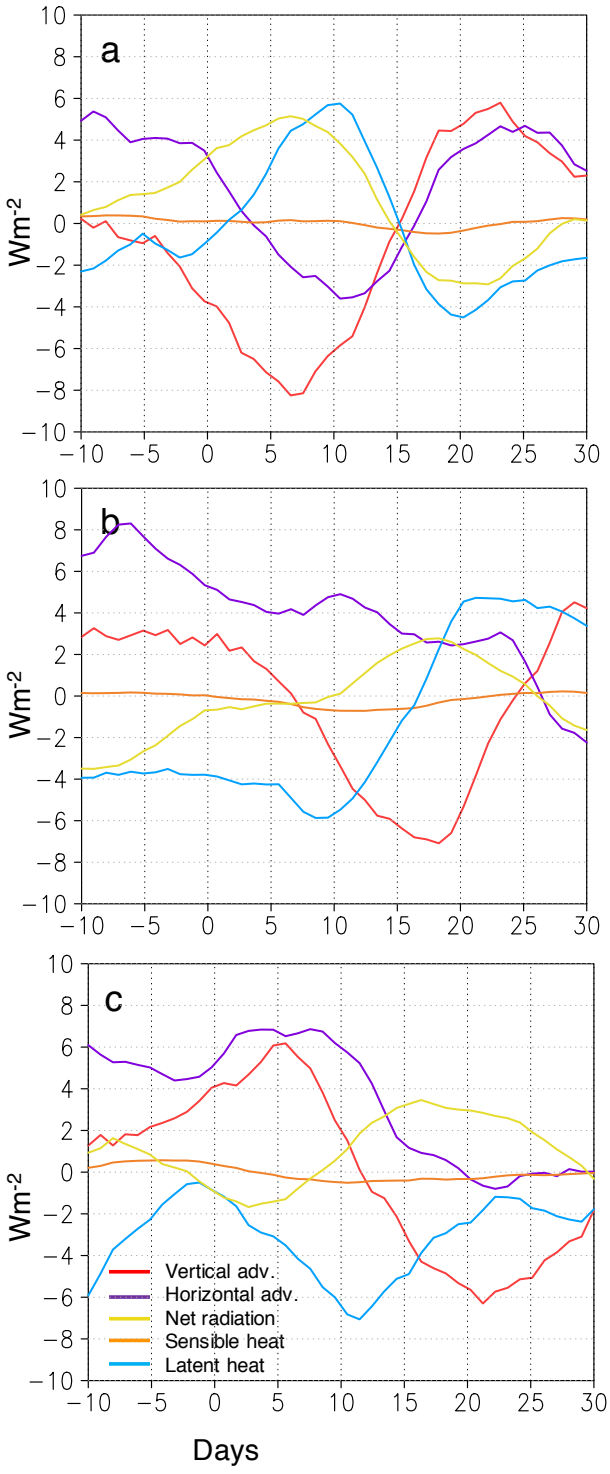

Figure 3.4: Time evolution of 11-day running mean MSE budget terms (Wm^{-2}) during the MJO for the IO (a), MC (b), and WP (c) regions. Colors signify vertical advection (red), horizontal advection (purple), net radiation (yellow), sensible heat (orange), and latent heat (blue). Day 0 was set as the day of initiation of the active phase of the MJO.

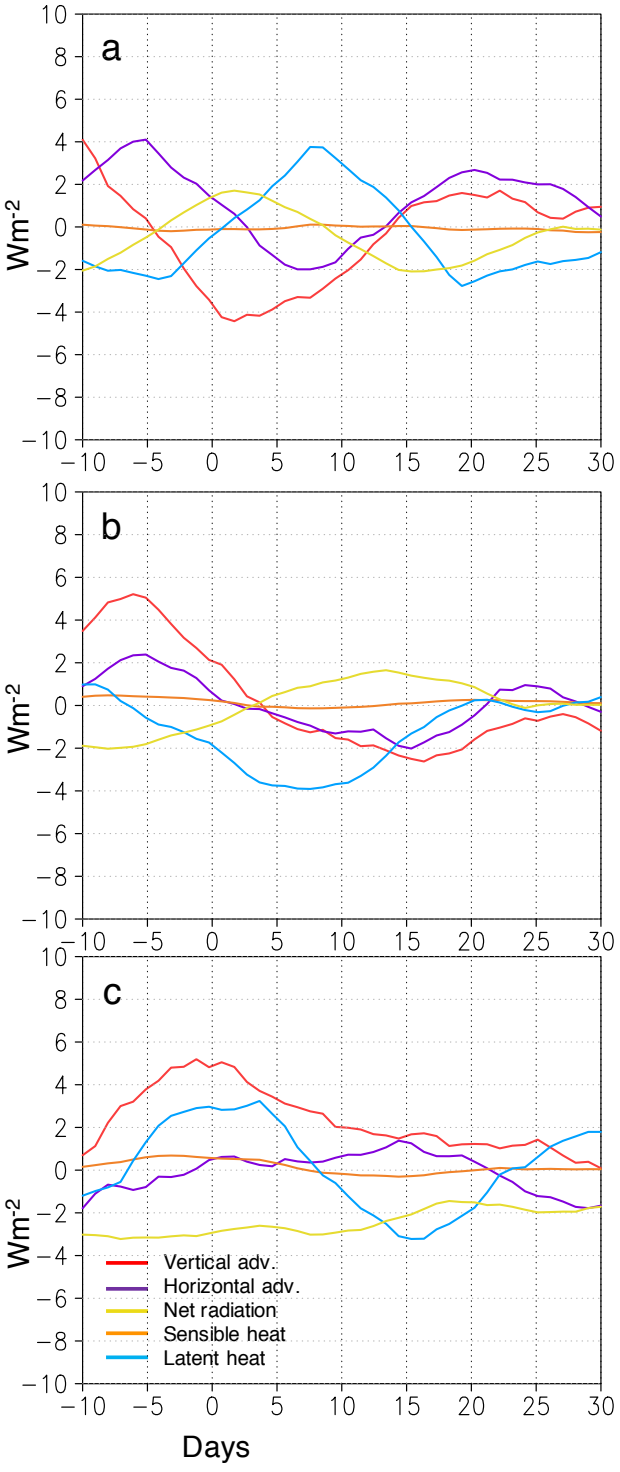

Figure 3.5: Time evolution of 11-day running mean MSE budget terms (Wm^{-2}) during IO-RCC for the IO (a), MC (b), and WP regions (c). Colors signify vertical advection (red), horizontal advection (purple), net radiation (yellow), sensible heat (orange), and latent heat (blue). Day 0 was set as the day of initiation of IO-RCC events.

signals remained consistent throughout the analysis period. That is, they were positive for the vertical advection term and negative for the net radiation term, which indicates weak convective activity. In relation to the weaker convective activity, the latent heat flux that followed the convective activity was also notably smaller. We also note that, as compared with the MJO, horizontal advection of the MSE was small prior to the convective initiation over the IO and was barely existent in the MC and WP. As a result, the IO-RCC convection initiated over conditions with a small buildup of MSE and moisture over the IO and MC, and no buildup of MSE over the WP (Fig. 3.6 b). The characteristics of the MSE budget terms show that although IO-RCC are events of convective activity that had a significant amplitude of RMM projection in phases 2-4, the nature of the convective activity is much shallower. This is indicated by the small magnitude of the vertical advection term, and the suggestion that convection is lacking large-scale circulation that strongly interacts with the large-scale environment.

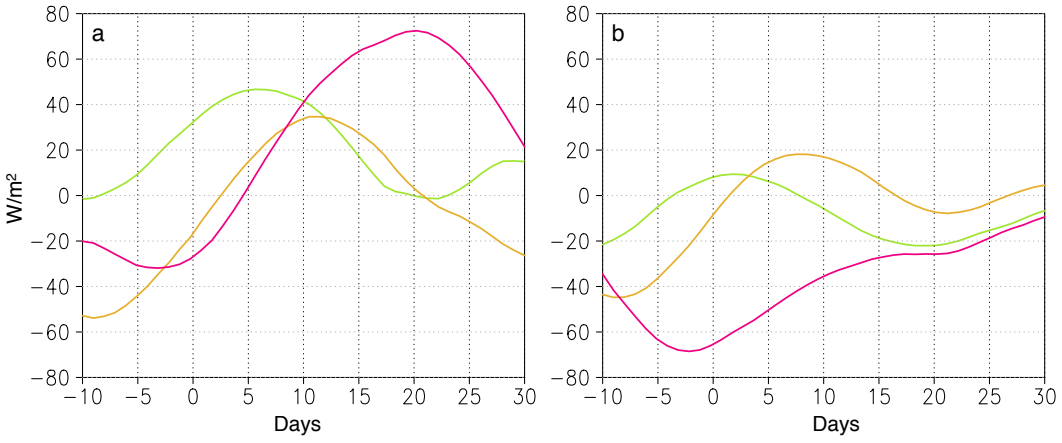

Figure 3.6: Time evolution of 11-day running mean column integrated MSE anomaly (Wm^{-2}) for MJO (a) and IO-RCC (b) for the IO (green), MC (orange), and WP (magenta) regions. Day 0 was set as the day of initiation of the active phase of MJO and IO-RCC events.

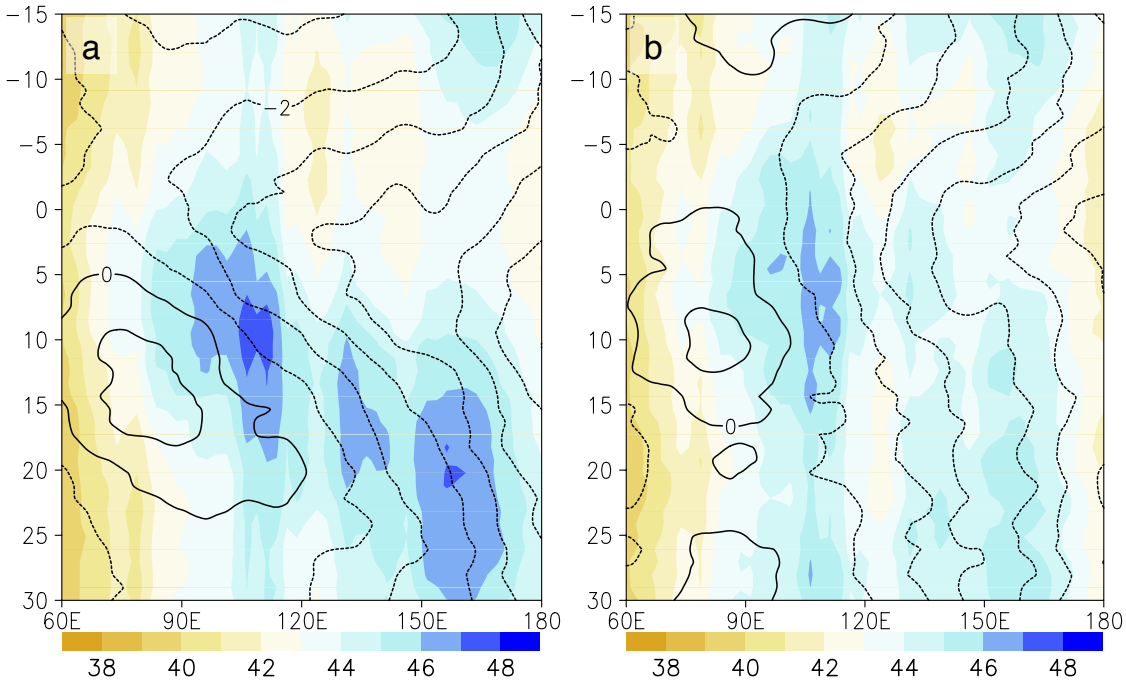

Figure 3.7: Composite Hovmöller of 15°S-15°N averaged U850 (contours; ms^{-1}) and precipitable water (color; kgm^{-2}) for the (a) MJO, and (b) IO-RCC.

The figure indicates that during MJO increased precipitable water developed eastward of the convective activities, but for the IO-RCC precipitation increase was limited westward of the MC. Furthermore, U850 pattern combined with the precipitable water distribution implies that during the MJO there was westward advection of moisture by the easterlies leading the MJO. Such supply of moisture was not available for the IO-RCC where the maximum precipitable water is taking place at the eastern edge of the IO.

3.3 Background SST during MJO and IO-RCC

SST fields associated with the MJO and IO-RCC were compared to investigate whether the background SST fields contributed to the differences in the MSE budget terms. SST variation at the MJO and longer timescale acts as a background SST field for convective activities that influence the large-scale MSE budget through its effects on surface moisture

flux and advection, and by inducing low-level convergence. With this in mind, composites of SST anomalies (SSTA) that occurred during the MJO and IO-RCC were made. The SSTA were separated into low and high frequency SSTA (LF-SSTA and HF-SSTA, respectively) fields to distinguish those signals at time-scales longer than the MJO from those at timescales comparable with the MJO (Figs. 3.8 and 3.9). LF-SSTA is defined as a 60 day low-pass filtered SSTA and HF-SSTA is defined as a 20-60 day band-pass filtered SSTA using a Lanczos filter (Duchon, 1979). 60 days was selected as the threshold between the LF-SSTA and HF-SSTA because MJO convection requires approximately 30 days to propagate from the IO to 180°E (Fig. 3.1).

Examination of the composite HF-SSTA showed that the MJO and IO-RCC were accompanied by a similar response in the SST to the preceding suppression and to the following convective activities (Fig. 3.8 a and 3.8 b). The HF-SSTA pattern was quite similar for both the MJO and IO-RCC. After initiation, at day 0, both the MJO and IO-RCC showed a common feature of negative SSTA spreading over the IO and a positive anomaly prevailing over the WP (Fig. 3.8 c and 3.8 d). However, the eastern edge of the MC at approximately 120°E, showed an opposite HF-SSTA sign between the MJO and IO-RCC, with the MJO having a positive SSTA. This is consistent with the finding that the center of convection shifted eastward for the IO-RCC as compared with the MJO; the signal of negative OLR of the IO-RCC extended to the eastern edge of the MC, where the opposite SSTA for the MJO was located (Fig. 3.3). A similar SST response to convective activity was apparent in the composite Hovmöller diagram for the HF-SSTAs of MJO and IO-RCC. Both showed increased SSTAs with the passage of the suppressed convective conditions from the IO to the WP and decreases in the anomaly as convection developed over the IO. Such responses by the ocean to the atmosphere is consistent with the ocean-

atmospheric feedback documented in previous studies (Shinoda et al., 1998; DeMott et al., 2015). Although the magnitude of the SSTA fluctuation was larger for the MJO, owing to its stronger and long-lasting convection, the overall pattern of HF-SSTA preceding and during convection over the IO was very similar to that of the IO-RCC. These results imply that the coupling of convection and the ocean is similar between MJO and IO-RCC. Therefore it follows that regarding the high frequency response, convective activity and suppression of the MJO and IO-RCC have similar effects on SSTs.

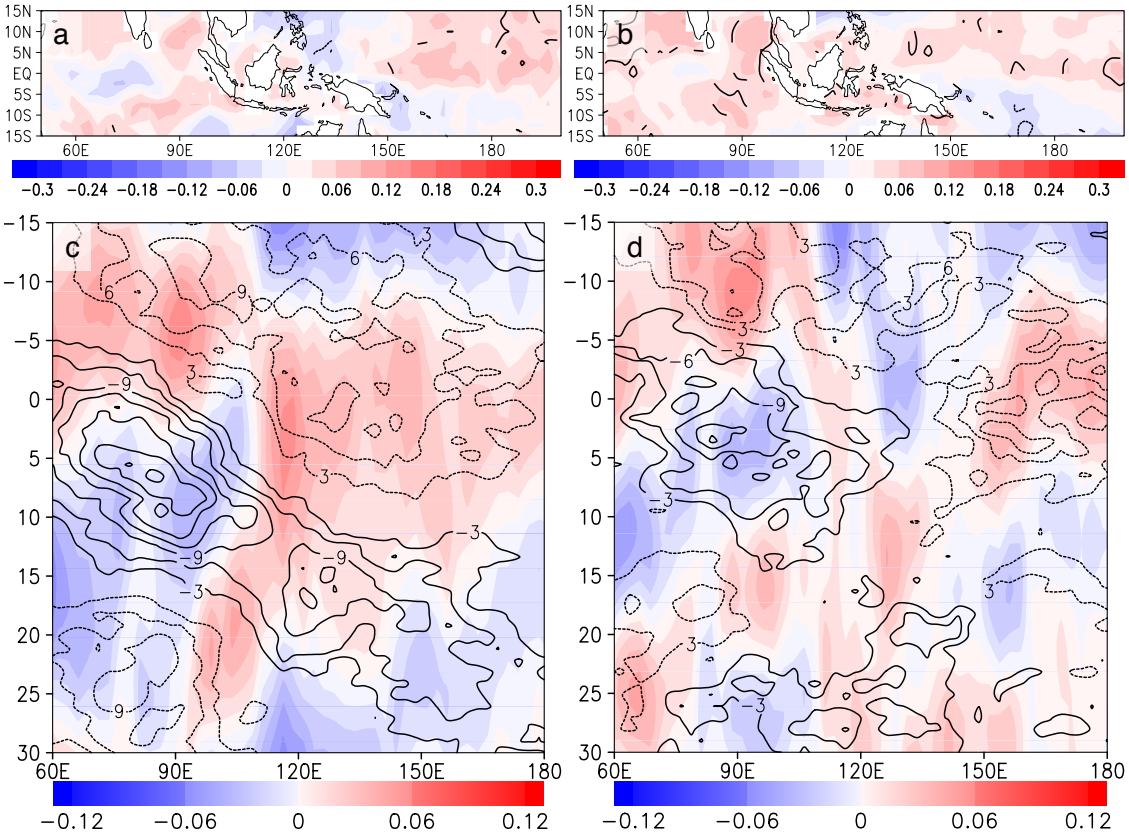

Figure 3.8: Composite of HF-SSTA at day 0 (top), and composite Hovmöller diagram of 15°S-15°N averaged HF-SSTA (shading; °C) and OLR anomalies (contour; bottom; Wm^{-2}) for the MJO (left) and IO-RCC (right). Contours on the day 0 composite (a and b) indicate statistically significant signal at 90%.

However, the MJO and IO-RCC are associated with strikingly different LF-SSTA fields (Fig. 3.9). At their initiation, the MJO and IO-RCC displayed a nearly reversed LF-SSTA

pattern from the eastern MC to the WP (Fig. 3.9 a and 3.9 b). A warm anomaly spread from the equatorial WP for the MJO, whereas a cold anomaly occurs for the IO-RCC. This contrast was the most distinct over the WP, where the positive and negative anomalies exhibited respective peaks for the MJO and IO-RCC. Although it was not as strong as over the WP, the MJO (IO-RCC) shows a positive (negative) LF-SSTA pattern over the IO as well. Moreover, both the MJO and IO-RCC showed a positive LF-SSTA field over the MC region. It is also noted that at the initiation of the MJO, an overall increase in the equatorial LF-SSTA occurred toward its peak over the WP. The different LF-SSTA patterns for the MJO and IO-RCC were also distinct in the Hovmöller composite of LF-SSTA (Fig. 3.9 c and 3.9 d). For the MJO, positive LF-SSTA began to prevail across the entire region from the IO to WP from approximately 10 days prior to initiation until the passage of the convective activity. In contrast, for the IO-RCC, the LF-SSTA was positive over the MC and negative elsewhere for almost the entire event duration, with the exception of a warm anomaly over the western IO before initiation. It is apparent that IO-RCC convective activities initiated over the IO, where the LF-SSTA is relatively warm at approximately 60°E, and spread eastward only up to the point at which the LF-SSTA reached its maximum at approximately 110°E. This result implies that although the MJO developed under conditions in which the buildup of moisture and MSE was supported by the eastward-increasing LF-SSTA pattern, a supply of moisture and buildup of MSE sufficient for development of convective activity into a large-scale system was not supported eastward of the MC during the IO-RCC owing to the negative LF-SSTA over the WP.

From the results of the LF-SSTA analysis, it is speculated that background conditions with an eastward increase of SST from the IO to the WP are important for the devel-

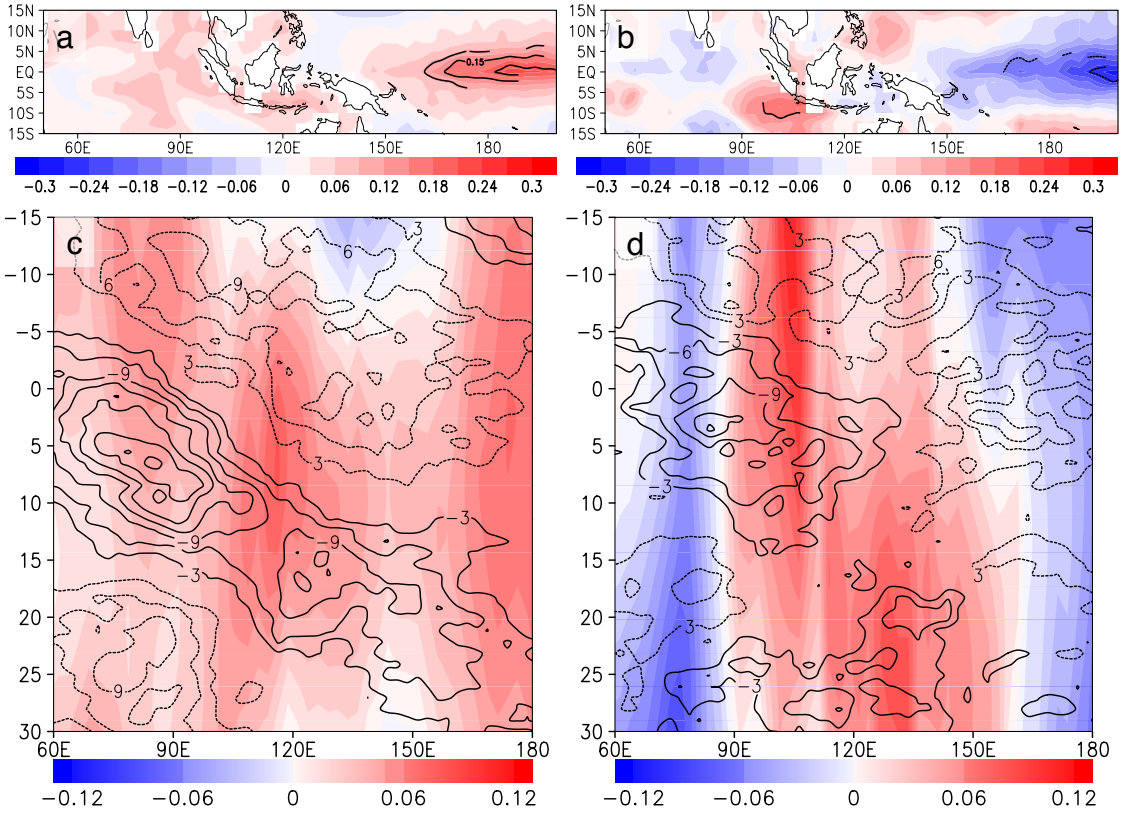

Figure 3.9: Composite of LF-SSTA at day 0 (top), and composite Hovmöller diagram of 15°S-15°N averaged LF-SSTA (shading; °C) and OLR anomalies (contour; bottom; Wm^{-2}) for the MJO (left) and IO-RCC (right). Contours on the day 0 composite (a and b) indicate statistically significant signal at 90%.

opment of MJO. The frequency of MJO events as a function of SST difference between the equatorial WP and IO was analyzed to provide statistical evidence for the importance of the zonal SST gradient on the MJO. The WP and IO regions are defined as the area within 120°E-180°E, 5°S-5°N and 60°E-120°E, 5°S-5°N, respectively, and the difference in area-averaged SST between the WP and IO is defined as a simple index of zonal SST gradient (WP-IO).

The frequency distribution of daily WP-IO during 1982-2012 binned by intervals of 0.4°C is shown in Fig. 3.10. The WP-IO peak was centered at 0.2°C, which is consistent with the climatological average of WP-IO at 0.3°C. With this in mind, histograms of the ratio of occurrence of MJO and IO-RCC sorted by the WP-IO value at their initiation

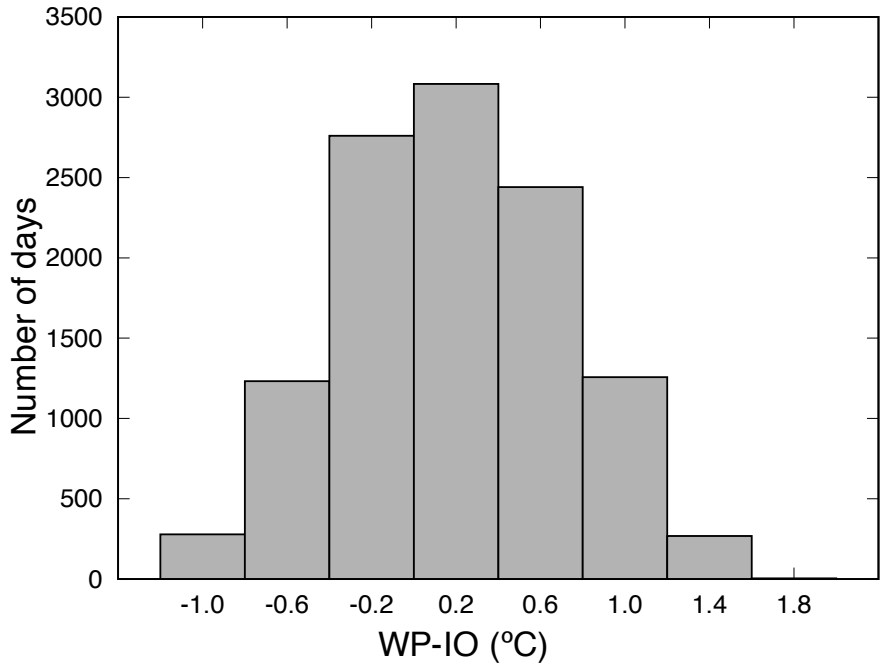

Figure 3.10: Histogram of area averaged SST difference of WP (5°S-5°N, 120°E-180°E) from IO (5°S-5°N, 60°E-120°E) in 1982-2012. Bins are at 0.4°C intervals with median values indicated at the bottom.

are shown in Fig. 3.11 a and 3.11 b, respectively. The value of WP-IO at the initiation is calculated from the average of WP-IO 10 days before the initiation of MJO or IO-RCC. It is apparent that, although MJO events were distributed around the mean WP-IO value with a slight negative skewness, the IO-RCC occurrences were concentrated at the mean. Considering the basic WP-IO frequency distribution, we normalized the number of MJO and IO-RCC events in each WP-IO bin by the number of days of WP-IO itself in each bin from 1982 to 2012. This shows the deviation of the MJO and IO-RCC frequency distribution from the frequency distribution of WP-IO. This normalized frequency distribution helped to clarify the actual influence of WP-IO on MJO and IO-RCC development. The normalized MJO frequency (Fig. 3.11 c and 3.11 d) increased with the WP-IO value, which indicated that the MJO tends to be more frequent when the WP-IO is higher. Conversely, the normalized frequency of the IO-RCC showed no

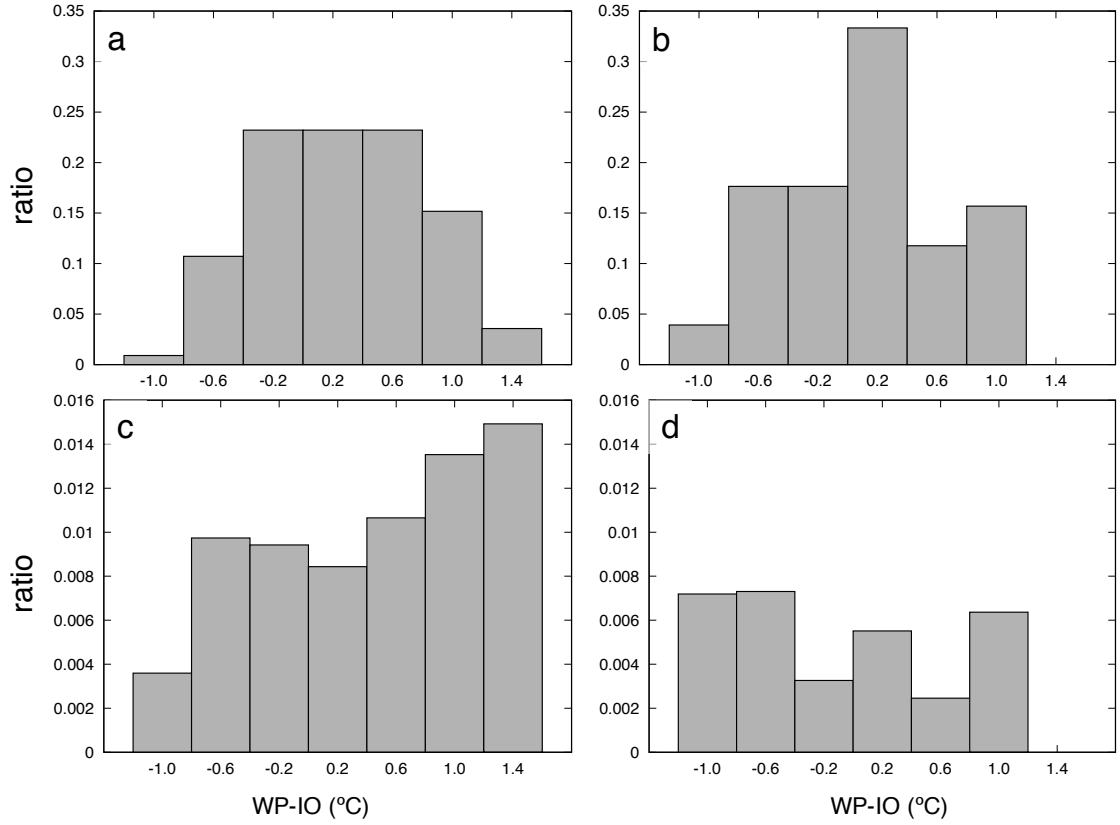

Figure 3.11: Ratio of occurrence of MJO (left) and IO-RCC (right) sorted by the WP SST-IO SST at their iniation (top) and normalized ratio by the total number of occurrences of WP-IO values between 1982 and 2012 (bottom).

consistent trend with the WP-IO and assumed a similar value across the range of the WP-IO.

It is conceivable that such a large-scale SST pattern is linked to interannual variability of the El Niño Southern Oscillation (ENSO; Trenberth, 1997) and El Niño Modoki (Weng et al., 2007). Regarding the ENSO, no significant bias was noted in the frequency of occurrence in the MJO or IO-RCC. Figure 3.12 shows the ratio of occurrence of MJO and IO-RCC for a given range of SSTA of the Niño 3.4 index. For both the MJO and IO-RCC, the peak was located around the center of the distribution of the Niño 3.4 index. The unevenness of the IO-RCC histogram is most likely attributed to the small sample size. Furthermore, the patterns of composite LF-SST for both the MJO and IO-RCC

were statistically insignificant eastward of 150°W (not shown), which indicates that the eastern Pacific SST is not dominant in modulating MJO or IO-RCC activities. In contrast, the MJO frequency of occurrence appears to be related to El Niño Modoki, which is associated with SSTAs over the central Pacific. The ratio of occurrence of MJO and IO-RCC for a given range of El Niño Modoki index (EMI; Ashok et al., 2007) are shown in Fig. 3.13 where EMI is defined as difference between the area averaged SSTA in the central Pacific (165°E-140°W, 10°S-10°N), and that in the eastern and WP (110-70°W, 15°S-5°N and 125-145°E, 10°S-20°N, respectively). The figure indicates that although the MJO tends to occur more frequently when the EMI is high, the occurrence of IO-RCC is apparently unaffected by the EMI. This result is consistent with the LF-SSTA analysis showing that positive SSTAs from the WP to central Pacific are favorable for MJO events, and El Niño Modoki can contribute to the formation of the LF-SSTA pattern associated with the MJO.

The frequency of MJO and IO-RCC occurrence in relation to the SST over IO were also investigated. Figure 3.14 show the ratio of MJO and IO-RCC occurrence by the area averaged SST over IO (5°S-5°S, 60°E-120°E) at their initiation. The histograms show that the frequency distributions were similar between MJO and IO-RCC with a positive skewness. For both MJO and IO-RCC, events occurred most frequently around 28.5°C, near the climatological value of IO (28.8 °C). The similarity of the two histograms implies that the SST over equatorial IO alone does not strongly influence whether a convective event develops into an MJO or not.

Further analysis was conducted to confirm that the SST pattern associated with the MJO, characterized by a spreading warm anomaly over the WP, is present in all seasons. A composite of the LF-SSTA for each season was made by categorizing MJO events ac-

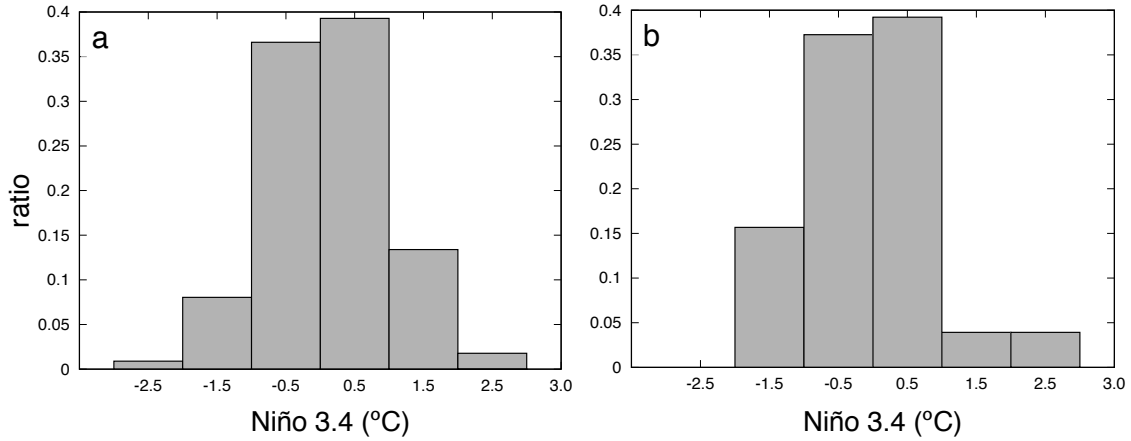

Figure 3.12: Ratio of MJO(a) and IO-RCC(b) occurrence according to the Niño 3.4 index value at their initiation. Bins are at 1.0°C intervals with median values indicated at the bottom.

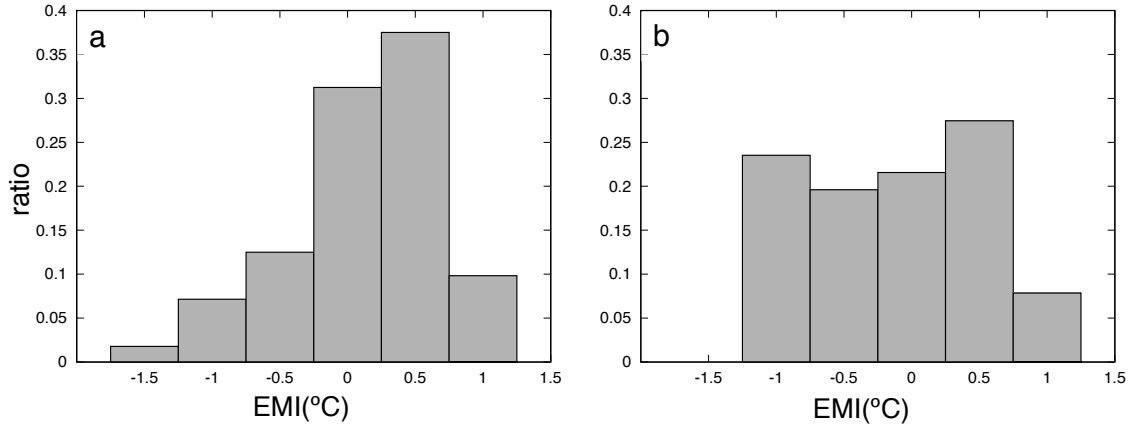

Figure 3.13: Ratio of MJO(a) and IO-RCC(b) occurrence according to the El Niño Modoki index value at their initiation.

cording to their initiation date, from December to February (DJF), March to May (MAM), June to August (JJA), and September to November (SON; Fig. 3.15). Seasonal differences were apparent, especially over the eastern edge of the MC, where LF-SSTAs are negative for DJF and MAM but positive for JJA and SON. However, we note that all seasons showed positive LF-SSTAs over the equatorial WP from 150°E to 180°E, where positive LF-SSTAs were found to be significant in an MJO composite of all events. Although some seasonal variations were noted, the overall results reinforce our view that high SST

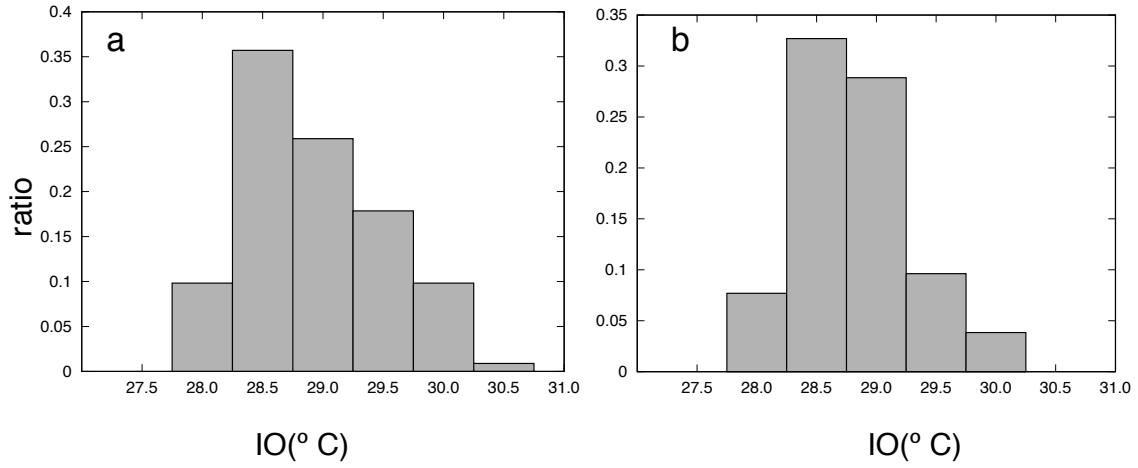

Figure 3.14: Ratio of MJO(left) and IO-RCC(right) occurrence according to the area averaged SST over IO (5°S-5°S, 60°E-120°E) at their initiation.

over the WP enhances MJO development.

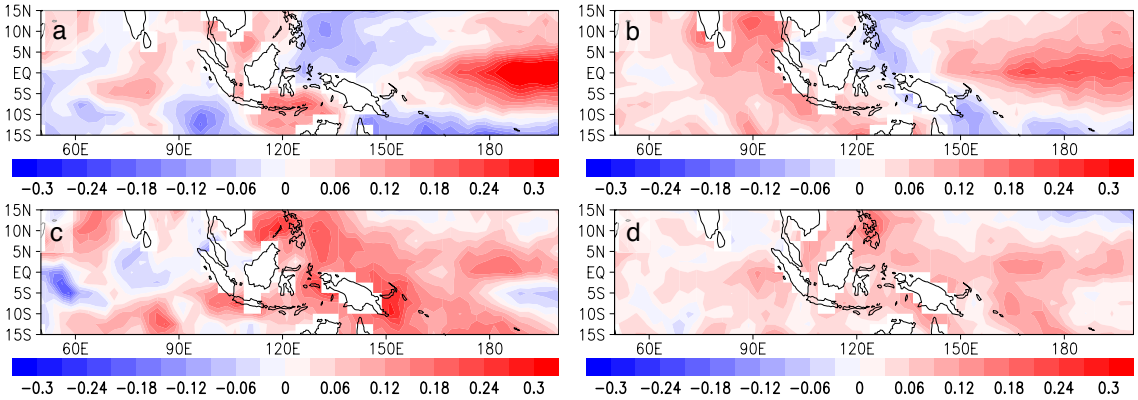

Figure 3.15: Composite of LF-SSTA at initiation of MJO during each season: (a) DJF, (b) MAM, (c) JJA, and (d) SON.

3.4 Summary and discussion

This chapter revealed MJO characteristics that distinguish them from tentatively organized convective events that fail to become an MJO. To identify these characteristics, days with a high RMM amplitude were classified into MJO and two types of RCC events by incorporating continuity into the RMM phase sequence. Two types of RCC were catego-

rized according to the location of the convective activity, in which IO-RCC and WP-RCC were associated with convective activity over the IO and WP, respectively. However, it was determined that WP-RCC was characterized by strong suppression over the IO and only weak convective activity over the WP. Therefore, WP-RCC events were not included in further analysis and comparisons between the MJO and IO-RCC were conducted. Although this simple classification method for MJO and RCC is by no means definitive, our findings demonstrated that the results are sufficient for distinguishing intraseasonal eastward propagating events as MJO and short-lived stagnant convective events as RCC. Intriguingly, comparison of the convectively suppressed state associated with the MJO and IO-RCC indicated that the intensity of the convective suppression preceding a convective event was not a critical factor in determining whether a convective event becomes an MJO. However, the MSE anomaly that developed in association with the circulation differed; convective activities of the MJO were preceded by a significant buildup of MSE and were accompanied by cooperative MSE flux and advective processes for convection. Such MSE accumulation processes were weak during the IO-RCC. Therefore, we infer that initiation of convection over an environment with the potential for MSE buildup is important for the development of an MJO. Thus, we investigated for such an MJO enhancing background through analysis of the SST. Analysis of different frequency SSTA fields showed that the LF-SSTA pattern distinguished the MJO from IO-RCC. Composites of the LF-SSTA showed contrasting patterns for the MJO and IO-RCC, in which they were associated with positive and negative SSTAs over the WP, respectively. Conversely, the HF-SSTA pattern, arising from changes in SST owing to air-sea interaction, showed a similar spatial and temporal evolution pattern for both the MJO and IO-RCC. Our results showed that as a function of a positive zonal SST gradient from IO to WP, the likelihood of

MJO occurrence rises with an increase in the zonal SST gradient. This positive zonal SST gradient could have contributed to the difference in the accumulation of the precipitable water during MJO and IO-RCC; i.e. the warmer water towards the WP should support greater build-up of precipitable water eastwards to the WP. This in turn would contribute to the build-up of MSE by westward horizontal MSE advection. Such processes were suggested to be important from the analysis of this chapter.

Hence, we infer that warming of the SST over the WP and generating a positive zonal SST gradient from the IO to the WP at timescales longer than intraseasonal is important for MJO development. However, how this background SST distribution influences the moist processes involved with the MJO needs closer examination with analysis on the background circulation driven by the background SST. The mechanisms for how the zonal SST gradient develop and are maintained also needs to be addressed in future work.

Chapter 4

Modulation of MJO propagation by zonal SST gradient

本章については５年以内に雑誌等での刊行予定のため、非公開。

Chapter 5

Analysis of MJO in NICAM-AMIP experiment

Reproducing the MJO in atmospheric models have been known to be notoriously difficult. NICAM is one of the few models which have seen some success in simulating the MJO (e.g., Miura et al., 2007; Miyakawa et al., 2014). However, due to the high computational cost of excluding cloud parameterization by computing cloud microphysical processes explicitly, NICAM simulations have often been restricted to relatively short simulations. The simulation on NICAM by Kodama et al. (2015) following atmospheric model intercomparison project (AMIP; Gates, 1992) protocol was a first climate simulation by NICAM using 14km mesh. The simulation spanned for over 30 years from 1 June 1978 to 31 December 2008 and enabled analysis on statistical properties of MJO and other atmospheric phenomena in NICAM for the first time (Kodama et al., 2015; Kikuchi et al., 2017). In this research, the methods used to analyze MJO events in the reanalysis data were applied to NICAM-AMIP simulation results. The analysis focused on evaluating the reproducibility of the relationship between MJO propagation speed and background environment in the NICAM-AMIP run. Following Kodama et al. (2015),

spin-up time of 7 months was taken and data starting from 1 January 1979 were used for this study. Differences in the analysis results between NCEP-NCAR Reanalysis data and NICAM-AMIP data will be discussed.

5.1 Detection of MJO events in NICAM-AMIP experiment

To analyze the properties of MJO simulated in NICAM-AMIP experiment, the method of MJO detection and tracking was applied to the NICAM-AMIP data. To calculate the RMM sequence, eigenvectors calculated from NCEP-NCAR Reanalysis1 data were used as in chapter 2 instead of using eigenvectors calculated from NICAM-AMIP data. Although the first two CEOF of OLR, U850, and U200 of the NICAM-AMIP data showed some resemblance to the structures of the CEOFs of the original WH04 (Fig. 5.1) when the order was reversed, there were also some notable differences. For example, there is a strong peak in OLR approximately at 60°W in CEOF2 which was not seen in either of the first two CEOFs of NCEP-NCAR data, implying that the amplitude of the variability of OLR over that region was higher than observed. It is also noted that the first two CEOFs calculated from NICAM-AMIP data only explained 15.0% and 14.2% of the variance where CEOFs calculated from NCEP-NCAR data explained 18.5% and 17.2%, respectively. These results were consistent with previous analysis on intraseasonal variability by Kikuchi et al. (2017), who showed that the structure of the CEOF calculated from boreal winter data of NICAM-AMIP showed a close resemblance to the CEOF calculated from observational data when the order of the first two CEOFs of NICAM-AMIP was reversed. It was determined that calculating the RMM sequence using the eigenvectors calculated

from NICAM-AMIP was not suitable for the purpose of this study since the objective was to assess the representation of MJO events as compared with the MJO in the real world. In calculating the RMM sequence, the projection of NICAM-AMIP data to first two CEOFs derived from NCEP-NCAR data was calculated. The trajectory of the projection of NICAM-AMIP data for the entire period of the analysis (May 1979 to August 2008) is shown in Fig. 5.2 along with the projection of NCEP-NCAR Reanalysis1 data for comparison. From the figure, the curvature of the RMM trajectory from NICAM-AMIP appears to be higher than that of NCEP-NCAR Reanalysis. This indicates the tendency of the RMM in NICAM-AMIP to fall more quickly than in reality. However, the amplitude of the RMM trajectory appears to be sufficiently at times to apply the method described in chapter 2 as is to detect MJO events in NICAM-AMIP simulation. It is also noted here that the method of MJO detection described in Kikuchi et al. (2017) applying bimodal intraseasonal oscillation index (ISO; Kikuchi et al., 2012) requires amplification of the amplitude of the index for NICAM-AMIP approximately by a factor of 2 since the amplitude is too weak to apply the method as is. The difference in the amplitude of the RMM index and the bimodal ISO index in NICAM-AMIP seems to be due to the difference in the variables used to construct the index. The bimodal ISO index uses only OLR, whereas RMM uses proxies of both convection (OLR) and circulation (U850 and U200). The inclusion of the circulation proxies should contribute to the higher amplitude of the RMM index since the structure of the CEOF of the circulation proxies was more similar to reality than the convection proxy (Fig.5.1; Kikuchi et al., 2017), and therefore should project better to the RMM derived from observational data than the OLR.

As a result of applying the methods of MJO detection described above, 51 events of MJO were detected in the period of the analysis. This amounts to the average of approxi-

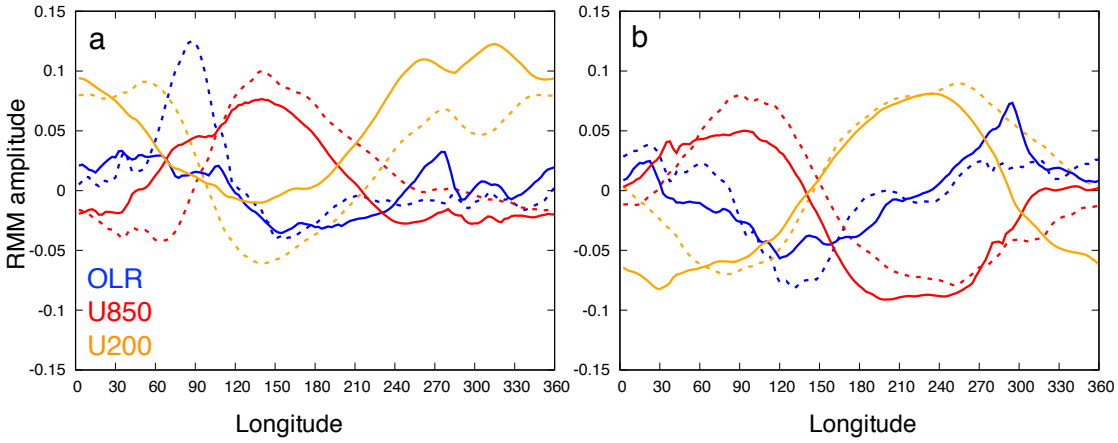

Figure 5.1: Structure of the first two CEOF, (a) CEOF1 and (b) CEOF2 of de-seasoned OLR (red), U850 (blue), and U200 (orange) of NICAM-AMIP simulation (solid line) and NCEP-NCAR (dotted-line). Note that CEOFs of NCEP-NCAR data are plotted together with CEOF1 and CEOF2 of NICAM-AMIP.

mately 1.7 events per year, which was smaller than the value of approximately 3.8 events per year in the analyzed NCEP-NCAR data. The cause of the difference in the occurring number of MJO events is investigated from the seasonality of MJO events. Figure 5.3 shows the distribution of MJO events during NICAM-AMIP simulation. In this analysis, the month of an MJO event was determined from the month of the average date between the first day of phase 2 and the last day of phase 7 of the event. The figure shows that the distribution of MJO events in NICAM-AMIP simulation was concentrated in late boreal winter with 58% of the events occurring from January to March. Conversely, MJO events were sparse during the boreal summer months and there were no MJO events during June, August, and September. The preference of MJO events to occur more in late boreal winter and less in boreal summer is consistent with the seasonality of frequency of MJO events in observation (Wang and Rui, 1990, Fig. 5.3 a). However, MJO occurrence in the real world is distributed much more evenly across the seasons; January to March MJO only accounted for 30% of the events, and 23 events occurred in June, August, and September together in NCEP-NCAR data. What were the causes of the biases in the seasonality of

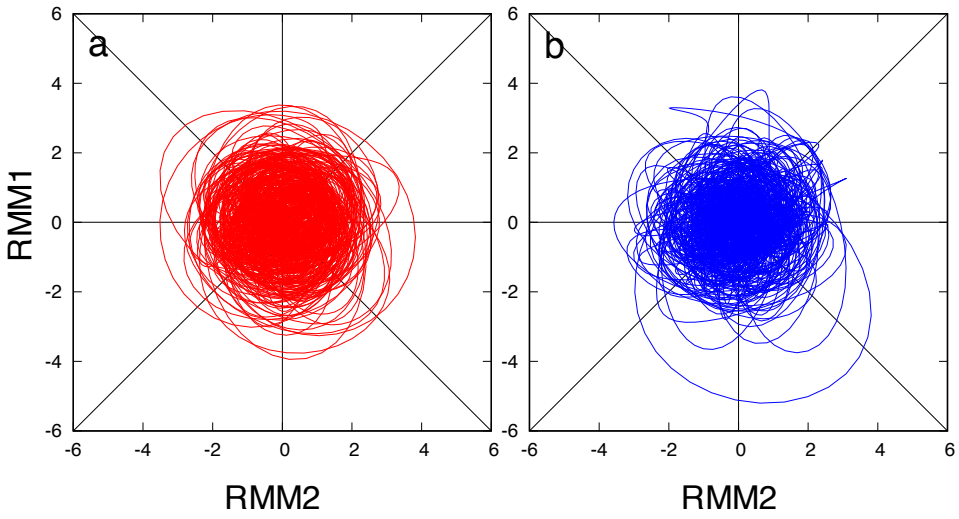

Figure 5.2: A trajectory of the RMM sequence from May 1979 to August 2008 for (a) NCEP-NCAR Reanalysis and (b) NICAM-AMIP data.

MJO occurrence, and the low number of events in total will be discussed in the following sections.

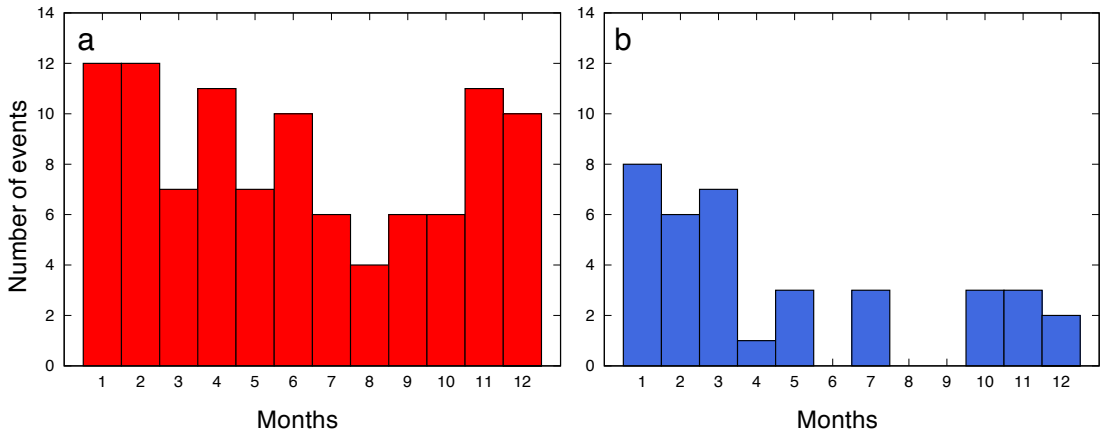

Figure 5.3: Histogram of occurrence of MJO events by the month for (a) NCEP-NCAR Reanalysis and (b) NICAM-AMIP data

5.2 Propagation speed of MJO in NICAM-AMIP simulation

Following the method in chapter 2, MJO propagation speed was tracked for each event in NICAM-AMIP. In the tracking, 13 events did not pass the t-test on the regression line and were not designated a propagation speed. 10 out of the 13 events had propagation speed ranging from 0 ms^{-1} to 2.5 ms^{-1}, and appeared to show no eastward propagation. The average propagation speed in NICAM-AMIP was 3.8 ms^{-1} which was slower than the 4.5 ms^{-1} in NCEP-NCAR data. Consistency between the MJO propagation speed and angular speed on RMM phase space was also checked accordingly, and one event was removed from the analysis due to the inconsistency between propagation speed and angular velocity. Figure 5.4 indicates that the propagation speed calculated from OLR tracking shows a linear relationship with the average angular speed from phase 2 to phase 7 of the event. In this way, MJO propagation speed was designated to 36 MJO events in NICAM-AMIP simulation, and further analysis on MJO was conducted on these 36 events. It is noted that the regression line of the plot of MJO propagation speed and angular velocity was almost parallel between NICAM-AMIP and NCEP-NCAR data. However, compared with the regression line of the NCEP-NCAR data, the regression line of the NICAM-AMIP was shifted downward indicating that the overall propagation speed in NICAM-AMIP was slower than in reality. This was also recognized in the histogram of MJO by their propagation speed (Fig. 5.5). The histogram shows that the distribution of MJO propagation speed in NICAM-AMIP was skewed towards slower events, and the bin of minimum propagation speed with MJO occurrence was lower than that of NCEP-NCAR Reanalysis data. The causes for the slowness of the MJO propagation speed in

NICAM-AMIP will be investigated and discussed in the following sections.

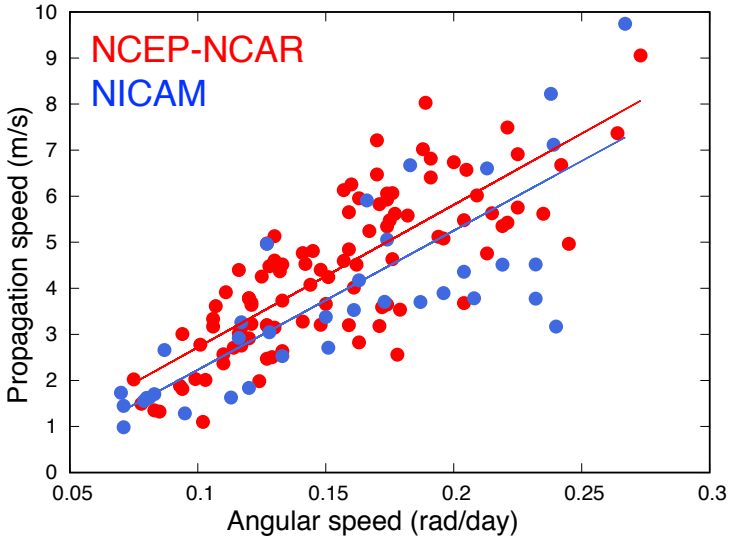

Figure 5.4: The propagation speed of MJO plotted against the angular speed of MJO events detected in NCEP-NCAR Reanalysis (red) and NICAM-AMIP (blue). The regression lines of the plots for each data set are also shown in their respective colors.

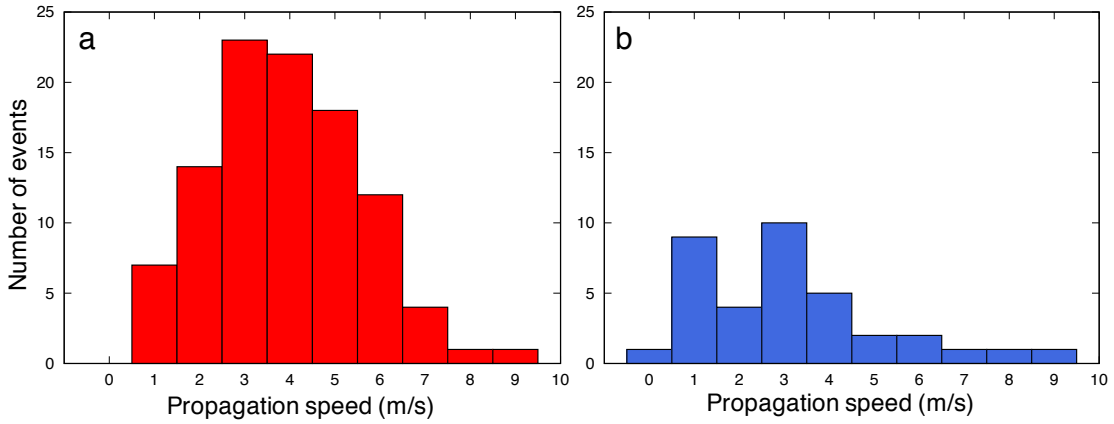

Figure 5.5: Histogram of occurrence of MJO events by their propagation speed for (a) NCEP-NCAR Reanalysis and (b) NICAM-AMIP data

5.3 Modulation of MJO propagation speed in NICAM-AMIP simulation

The relationship of MJO propagation speed and zonal SST gradient from IO to WP was examined in the same way as described in chapter 3. Figure5.6 shows MJO propagation speed plotted against the WP-IO defined in the previous chapter as an index of zonal SST gradient between IO and WP. It appears from the plot that MJO propagation speed and WP-IO do not show much correlation. However, when the boreal winter events, defined here as MJO events that occurred between December and April, were examined by themselves, the correlation increases to -0.44, close to the value shown by the MJO events in NCEP-NCAR data. It is noted though that the relationship between propagation speed and WP-IO of the winter events appears to be tilted towards slower propagation speed than in the NCEP-NCAR plot. Therefore, slower MJO was associated with given WP-IO in the NICAM-AMIP simulation than in reality.

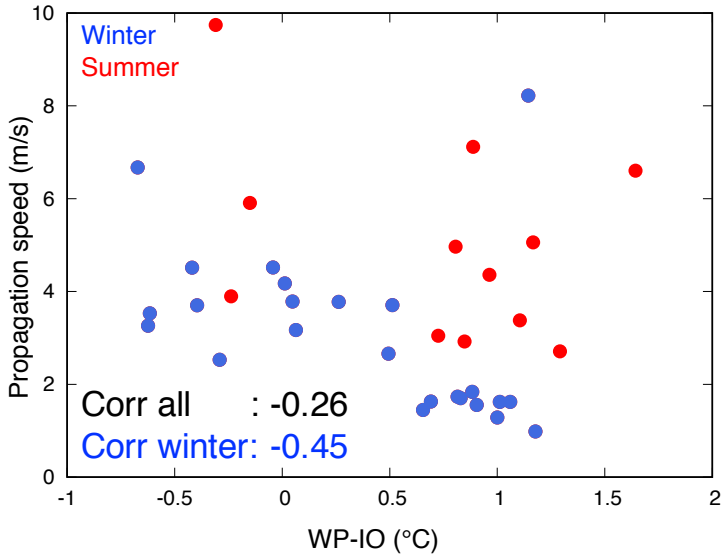

Figure 5.6: Scatter plot of MJO propagation speed (ms^{-1}) and WP-IO (°C). The events during boreal winter and summer are colored blue and red, respectively.

Furthermore, MJO propagation speed of events in boreal winter and LF-U850 over MC in NICAM-AMIP simulation also showed a negative correlation (-0.43) with each other (Fig. 5.7). This result was consistent with the relationship found between propagation speed and LF-U850 in the reanalysis data. However, as with the correlation between propagation speed and WP-IO index, the correlation drops to -0.29 if the summer events are included in the analysis.

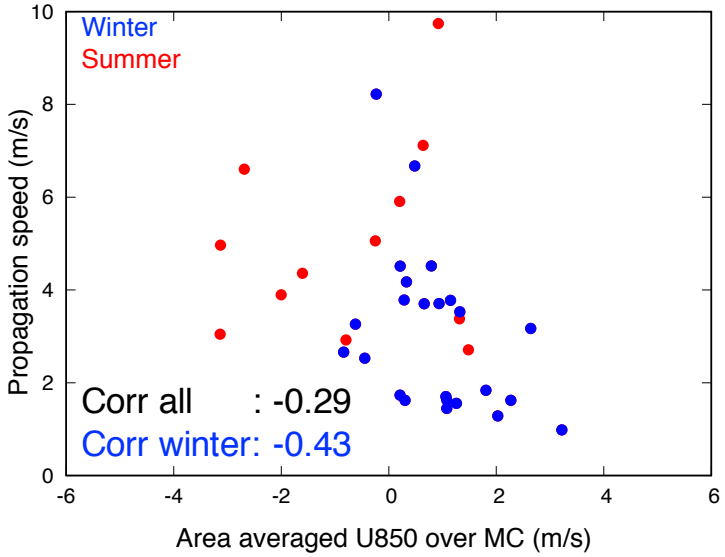

Figure 5.7: Scatter plot of MJO propagation speed (ms^{-1}) and LF-U850 over MC. The events during boreal winter and summer are colored blue and red, respectively.

The results of this analysis on NICAM-AMIP MJO interestingly showed consistency with the analysis on MJO in the real world which indicated slowing of the MJO with the intensification of zonal circulation driven by the zonal SST gradient for the boreal winter MJO events. However, slow bias was present in all of the analysis including analyses restricted to boreal winter events. Also intriguingly, a decrease in the correlation between propagation speed with WP-IO and LF-U850 was observed in the boreal summer season when MJO events tended to be undetected by the applied method. Possible causes for the slow bias in the boreal winter events and discrepancies found in the boreal summer events

with the results from analysis on real-world MJO will be discussed in the next section.

5.4 Discussions and summary

5.4.1 Slow bias of MJO propagation speed in NICAM-AMIP simulation

The results of the last section indicated a systematic slow bias in the simulated MJO in NICAM-AMIP run. The sluggish propagation of MJO convection was recognized from the composite Hovmöller diagram of OLR for 10 slowest MJO events (Fig. 5.8). There was persistent convective activity over the MC in the whole duration of the slow MJO, and it appeared that rather than propagating eastward, convective activity seemed to spread its active region eastward to approximately the dateline. The average duration and propagation speed of the active phase of the slow events in NICAM-AMIP was 58 days and 1.5 ms^{-1} respectively. The duration was longer compared to 44 days, and speed was slower compared to 1.7 ms^{-1} for the slow MJO of NCEP-NCAR Reanalysis. It was also noted that the occurrence of slow MJO events in NICAM-AMIP simulation was highly biased to January, with 8 out of 10 of the slow MJO occurring in January. The other two events were in February and March. In comparison, slow MJO events in NCEP-NCAR Reanalysis occurred between September to February, with a slight preference to February with the occurrence of 4 events.

Following the protocol of AMIP, sea surface condition was given in NICAM-AMIP simulation by nudging SST and sea ice to the monthly mean value of Hadley Centre Sea Ice and Sea Surface Temperature data (Rayner et al., 2003) using a slab ocean model. Therefore, it is unlikely that there are large biases in the SST fields especially in long

time-scale which was found to influence the behavior of MJO propagation. Thus biases over land and circulation were examined.

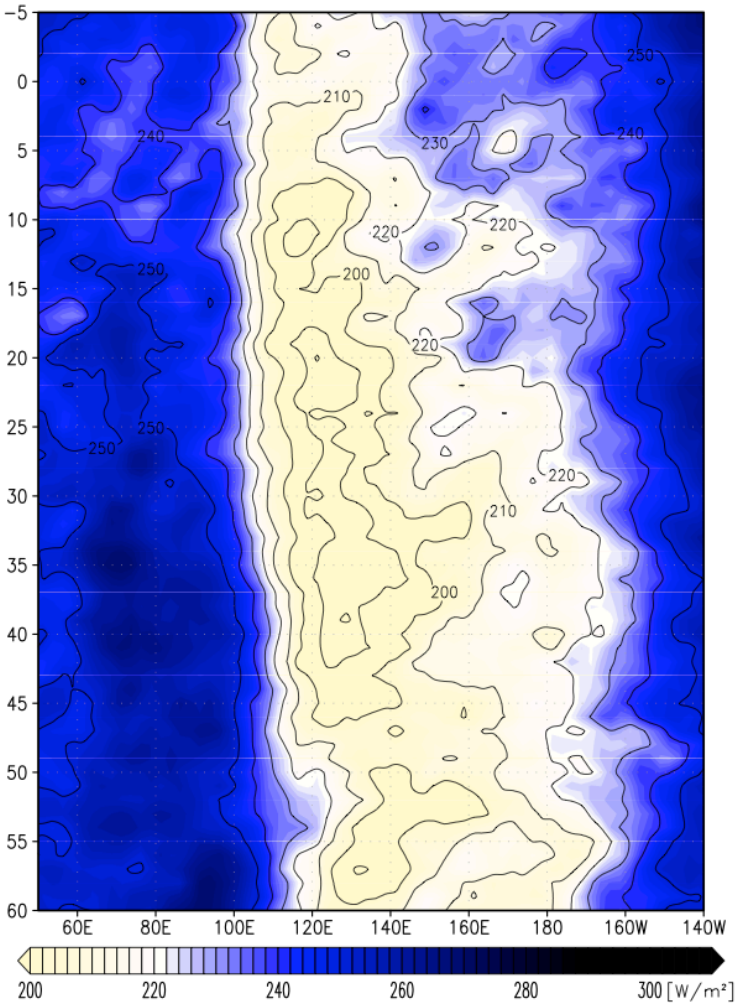

Figure 5.8: Composite Hovmöller of 15°S-15°N averaged OLR of the slow MJO in NICAM-AMIP simulation.

Taking note that slow MJO events were concentrated in January, the climatology of low-level winds and ground temperature during boreal winter were examined and compared with the climatology in NCEP-NCAR Reanalysis. Figure 5.9 shows the three months mean of 850 hPa horizontal winds and surface temperature from January to March of the 30-year climatology of NCEP-NCAR Reanalysis and NICAM-AMIP simulation. For the NCEP-NCAR Reanalysis, 3 months climatology of skin temperature was used to compare

with the ground temperature of NICAM-AMIP since it was the closest available temperature product to ground temperature. Comparing the two climatologies, it was noticed that the ground temperature of NICAM-AMIP over Australia was much higher than the skin temperature over the same area in the reanalysis data. The difference reached close to 10°C in the wide region over central Australia. The cause for the high ground temperature bias has been identified as a fault in the model setting in which sulfate aerosols were transparent to radiation (Miura, 2018, personal communication). Another noticeable difference was identified in the low-level westerlies over the MC. Comparison of the westerlies in Fig. 5.9 between NICAM-AMIP and reanalysis indicated stronger westerlies across the MC for NICAM-AMIP. The westerlies were almost as twice as strong as the westerlies in the NCEP-NCAR climatology, around where the climatological westerlies took their maximum, from approximately 120° to 140°E. Taken together, it appeared that the Australian Summer Monsoon, characterized by westerlies over the MC (Kajikawa et al., 2009), was unrealistically strong in the NICAM-AMIP simulation due to the high ground temperature over Australia.

The climatological ground temperature and the zonal wind over the MC appeared to take unrealistic values as consequences of unrealistic setting in the model physics. However, the systematic tendency of MJO propagation speed to be slower in NICAM-AMIP under stronger climatological westerlies over MC was interestingly consistent with the results of the previous chapter. It was also intriguing that MJO propagation speed appeared to be modulated in two scales; systematic slowing of MJO events by stronger climatological westerlies over the MC, and modulation of the variation of MJO propagation speed within NICAM-AMIP simulation so that they are still negatively correlated with the zonal SST gradient and the strength of the low-level westerlies over the MC.

It was also noted that with the systematic slowing of the MJO in boreal winter, duration of MJO events had become longer. Many of the boreal winter MJO events in NICAM-AMIP spanned for nearly two months from January to February. In contrast, most of the MJO events in the real world only lasted for one to 1.5 months. As a result, MJO events could not develop as frequently as they did in the real world since MJO events usually only develop one at a time and lengthening of an event will lead to the later initiation of the subsequent event.

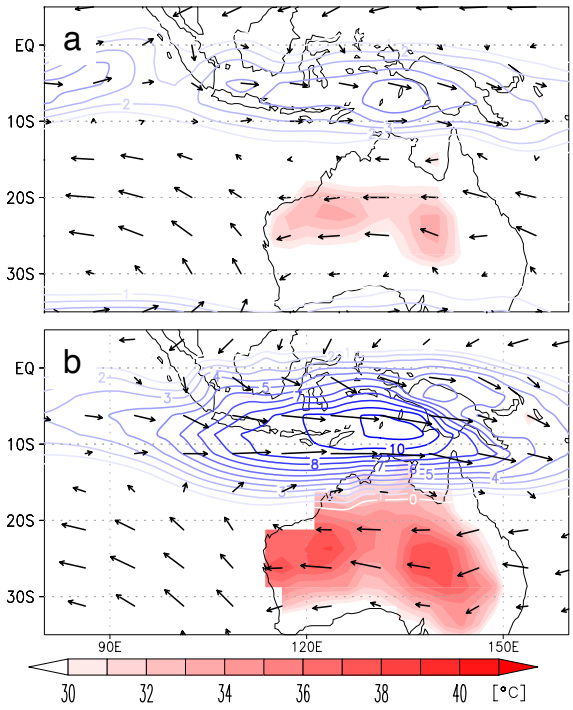

Figure 5.9: January to March climatology of 850 hPa winds (vectors) with the region of westerlies contoured, and surface temperature (color; °C), for (a) NCEP-NCAR Reanalysis and (b) NICAM-AMIP reanalysis data. The surface temperatures for NCEP-NCAR Reanalysis is skin temperature, and for NICAM-AMIP is the ground temperature.

Causes for the deficit of MJO events in the boreal summer months were also investigated from a comparison of the 30-year climatology of atmospheric conditions during those months. As in the analysis in the previous section, three months climatology from June to August of surface temperature (°C) and 850 hPa zonal winds are shown for NCEP-

NCAR Reanalysis and NICAM-AMIP simulation (Figs.5.10 a, b). Here again, the skin temperature of NCEP-NCAR Reanalysis was used to compare surface temperatures with NICAM-AMIP run. Likewise with the temperature over Australia in the boreal winter, the climatology of ground temperature was much higher in NICAM-AMIP run than in reanalysis data. This was especially noticeable over the Arabian Penninsula where climatology of ground temperature reached above 40 °C in the northeastern parts of the peninsula. There were also noticeable differences in the 850 hPa winds between NICAM-AMIP and reanalysis. The horizontal winds over the Arabian Sea had a stronger meridional component in the NICAM-AMIP simulation, and the location of the westerlies had stronger northward tilt from the eastern tip of Somalia to Pakistan. The region of strong westerlies in the reanalysis data only reached northward approximately to the southern border of Pakistan. The location of maximum westerlies was also shifted northward for NICAM-AMIP over the Bay of Bengal. It appeared from the figure that there was a slight change in the course of the Indian summer monsoon (Fieux and Stommel, 1977) in the NICAM-AMIP simulation.

Following the analysis of the surface temperature and low-level winds, the climatological location of deep convection during the boreal summer months was investigated from OLR. Figure 5.10 c and d show the three months climatology from June to August of OLR, with 850 hPa winds as in Figs. 5.10 a and b. The figure shows that while the location of minimum OLR takes place around the eastern edge of the Bay of Bengal in the reanalysis data, it is shifted northward to India and Bangladesh in NICAM-AMIP run. The northward shift of the OLR minimum during the boreal summer months in NICAM-AMIP implies a further northward shift of boreal summer MJO events. This would cause MJO events to be undetected in the current MJO detection method since RMM projection

is made on 15°S-15°N averaged OLR and is consistent with the small number of MJO events during boreal summer in NICAM-AMIP simulation. If this is the case, a different method will be required for further investigation of intraseasonal variability during boreal summer in NICAM-AMIP run.

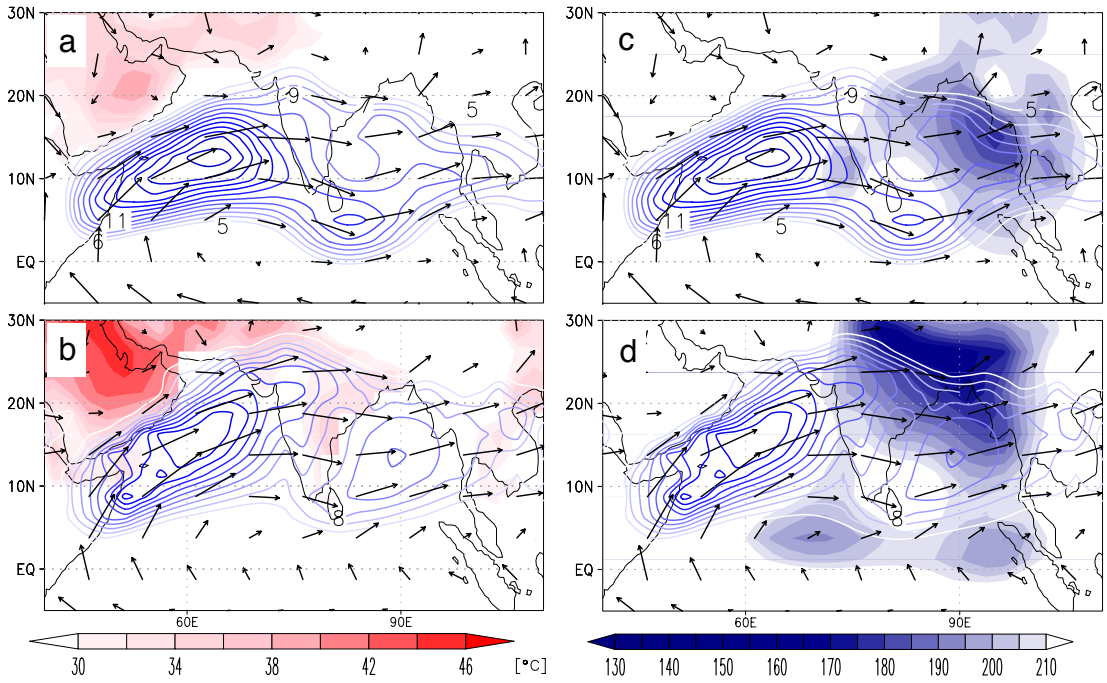

Figure 5.10: June to August climatology of 850 hPa winds (vectors) with region of westerlies greater than 5 ms^{-1} contoured, surface temperature (color in red shades; °C) and OLR (June to August climatology of 850 hPa winds (vectors) with region of westerlies greater than 5 ms^{-1} contoured, surface temperature (color in red shades; °C) and OLR (color in blue shades; Wm^{-2}) for (a and c) NCEP-NCAR Reanalysis data and (b and d) NICAM-AMIP data. The surface temperatures for NCEP-NCAR Reanalysis is the skin temperature, and for NICAM-AMIP is the ground temperature.

5.4.2 Summary

In summary, MJO events were detected in NICAM-AMIP simulation data using the same RMM methods as in reanalysis data, and their properties with the MJO in the real world were compared. The number of detected MJO events was smaller in NICAM-

AMIP, and it was attributed to two systematic biases within the simulation. The first was, due to the northward shift of the location of the climatological minimum of OLR during boreal summer, MJO events during boreal summer tended to be undetected using the RMM. The second was thought to be from the systematic slow bias in the propagation speed in boreal winter; slower MJO events were longer in duration, and the number of events within one boreal winter season decreased.

Despite these biases, MJO in NICAM-AMIP simulation interestingly displayed a consistent relationship between MJO propagation speed and environmental fields as the observation. Although the correlation was weaker than in reanalysis data, MJO propagation speed was negatively correlated with both the indices of the zonal SST gradient and zonal circulation strength. The reproduced relation of the MJO propagation speed and background fields and the systematic slow bias of MJO propagation speed was consistent with other analysis which pointed to the slowing of the MJO with the intensification of the large-scale zonal circulation. It also showed modulation of MJO propagation at two levels, which may reflect the modulation of MJO propagation speed occurring at two different scales. However, more evidence to support this view is needed to make this argument and will be a topic for future research.

Chapter 6

Summary and general conclusions

6.1 Summary and discussions

This study motivated by the notion that MJO may be explained as a forced response from the large-scale environment has revealed some intriguing relationship between MJO and background states in which they occur.

Investigation on the environment supporting MJO development was conducted from a comparison of MJO and other tentative convective events, RCC, which was classified by constructing a classification method of convective activities. Contrary to some preexisting results (Hirata et al., 2013; Kim et al., 2014), this analysis showed that even when preceded by a major convective suppression event, convective events did not develop into an MJO when a large-scale buildup of MSE was inhibited. The difference in the MSE accumulation between MJO and RCC was related to the contrasting low-frequency basic state SST pattern; the MJO and RCC events were associated with anomalously warm and cold low-frequency SSTs prevailing over the western to central Pacific, respectively. Differences in the SST anomaly field were absent from the intraseasonal frequency range of 20-60 days. The basic state SST pattern associated with the MJO was characterized by a

positive zonal SST gradient from the IO to the WP, which provided a long-standing condition that allowed for sufficient buildup of MSE across the IO to the WP via large-scale low-level convergence over intraseasonal and longer timescales. The results suggested the importance of such basic state SST, with a long-lasting positive zonal SST gradient, for enhancing convection over a longer than intraseasonal timescale to realize a complete MJO lifecycle.

On the basis of the findings in chapter 3, GCMs in the absence of air-sea coupling should have the potential to reproduce the MJO as long as the prescribed SST is favorable for MJO development. This inference is supported by the fact that some GCMs are capable of simulating MJO-like disturbances if observed or climatological mean SSTs are given and that their representations are improved by air-sea coupling (e.g., Inness and Slingo, 2003; Benedict and Randall, 2011; Klingaman and Woolnough, 2014; DeMott et al., 2014). Furthermore, the basic-state SST field that was considered essential was on a timescale much longer than that of MJO and was not a product of SST response to convective suppression (Shinoda et al., 1998). However, changes in the HF-SSTA from air-sea coupling can supplement the MJO supportive background SSTs within an MJO timescale, as reported by Flatau et al. (1997) and Hirata et al. (2013). Therefore, although the results of this study indicate the dominant influence of LF-SSTA over that of HF-SSTA on MJO development, findings of this study do not conflict with their work and others (e.g., Hendon et al., 1999; Klingaman and Woolnough, 2014). Slowly changing SST is an influential environmental factor for the MJO because it can provide a near-standing bottom boundary condition for the atmosphere on an intraseasonal timescale. For example, episodes of interannual variability such as positive ENSO and positive IOD modes tend to produce faster MJO events (Izumo et al., 2010; Pohl and Matthews, 2007) and

vice versa. Prior research has indicated that MJO events occur more frequently, and are enhanced during negative IOD events (Ling et al., 2013; Shinoda and Han, 2005; Izumo et al., 2010) and after La Niña evens (Pohl and Matthews, 2007). Complementary to these studies, the present study proposes that background SSTs with a positive zonal SST gradient toward the WP from the IO play a fundamental role in developing the MJO by inducing low-level equatorial westerlies, as shown by the one-layer model of Lindzen and Nigam (1987). Observational evidence that MJO activity peaks with the season and location of mean low-level westerlies (Zhang and Dong, 2004), and model dependency on simulating mean westerly winds correctly for simulating MJO (Inness et al., 2003) also corroborate with the results presented here.

It should also be noted that the overall positive LF-SSTA across the IO to the WP associated with the MJO contributes to a potential for the necessary large-scale buildup of MSE to maintain active convection on an intraseasonal timescale. The positive zonal SST gradient toward the WP also contributes to MJO propagation in that it enables greater MSE buildup on the eastern regions. Such an effect was recognized from the subsequent analysis on how MJO propagation speed is affected by the background SST. This was done by constructing a tracking method of MJO propagation and comparing the background states that MJO occurred in by their propagation speed. Analysis on the fastest and the slowest 10 MJO events revealed differences in the moist processes that occurred during each of the MJO group. MSE budget analysis showed that long-lasting deep convection develops across IO region to the WP region for the slow MJO with preceding build-up of MSE from horizontal advection, and positive feedback to convection from latent and radiative heating terms. On the other hand, for the fast MJO, deep convection developed only for about 10 days and buildup of MSE build-up before convection and positive feedback to

convection occurred only over the IO region. These results indicated that in slow MJO development of convective activity continued until the MJO passed the MC, while the fast counterpart appeared to merely consume accumulated MSE as it propagated eastward.

The differences in the accompanied moist processes in slow and fast MJO were associated with different oceanic states that they occur in; the slower events were associated with the condition of LF-SST distribution with a positive zonal gradient from the IO to WP. LF-SST associated with fast MJO was much the same across IO to WP. Significant differences in the SST pattern were not recognized in the intraseasonal timescale of 20-60 days. Furthermore, an extension of the analysis of propagation speed to rest of the events revealed that the relationship between zonal SST gradient and propagation speed is not a trend restricted to the fastest and the slowest groups but is an overall relationship that is displayed by all of the events. Taking note that the presence of zonal SST gradient in low-frequency range has the potential to enhance large-scale zonal circulation, the component of the zonal wind associated with the background circulation was also analyzed. The analysis showed that there is a tendency for MJO to propagate slower when the background large-scale zonal circulation was stronger, implying that slower MJO is involved with enhancement of large-scale zonal circulation.

These results presented new perspectives on the MJO propagation since they challenge the eastward propagation mechanism of the moisture mode theory (Sobel and Maloney, 2012, 2013). While moisture advection appeared to be important for MJO development, MJO propagation itself should not be explained by advection of moisture if propagation speed was negatively correlated with background low-level westerlies. Moreover, contrasting characteristics of the slow and fast MJO, taken together with the continuous spectrum of MJO events in propagation speed casts doubt on the belief that MJO should

be explained as a distinct mode of the atmosphere with single propagation mechanism.

Following the analysis on real-world MJO, the reproducibility of such relationship of MJO properties with the background fields in the model simulation was investigated using climate simulation data from NICAM-AMIP run. It was found that although the simulated MJO events tended to be slower than reality and are biased in the season of their occurrence to late winter, the tendency of MJO to be slower under a condition with higher SST in the WP than the IO was also reproduced in NICAM-AMIP simulation. The causes for the systematic slow bias and decrease in the number of boreal summer MJO were related to the difference in monsoonal circulation in the NICAM-AMIP run. Although it appeared that the strength of the background circulation related to MJO propagation speed was being modulated by different reasons than in reality, MJO in NICAM-AMIP simulation still showed a relationship with the background environment that was in agreement with the relationship observed with the real world MJO. Sensitivity studies on MJO development and propagation that test these relationships are part of the future work that is expected to provide further insight into the nature of the MJO.

6.2 General conclusions

In conclusion, this study identified characteristics of the MJO that distinguishes them from other tentative convective activities in the differences in the MSE build-up processes. Such differences were related to the low-frequency SST pattern, in which MJO was associated with SST with a positive zonal gradient from IO to the WP. Investigation of how such SST pattern affects the MJO properties showed that MJO propagation speed becomes slower as the zonal SST gradient increases, and large-scale zonal circulation is enhanced in both observation and in NICAM-AMIP simulation. The results of this study

indicated the importance of the influence of the low-frequency SST on the MJO and implied that MJO exists as part of the large-scale circulation driven by the low-frequency SST pattern.

Acknowledgement

I would first like to thank my advisor Associate Prof. Hiroaki Miura for all that he have taught me over the years and for patiently supporting my time consuming progress. I am also thankful to Prof. Masaki Satoh, Prof. Yukari Takayabu, Prof. Yukio Masumoto, and Associate Prof. Tomoki Tozuka for undertaking the referee.

I have also benefited much from the opportunity to be a research student at JAMSTEC and aboarding R.V. Mirai during pre-YMC observation campaign. Dr. Satoru Yokoi and Dr. Kunio Yoneyama have provided me with necessary guidance during the experiences there.

Earth and Planetary Science Department office of the School of Science, the University of Tokyo have kindly provied assistance in the multitude of office work that came along in the course of the research activities, and members of the Atmospheric and Oceanic Science Group have provided a helpful environment to work in.

I am also obliged to the University of Tokyo, Divison for Counselling and Support for the support from the student counselling team. I am especially thankful to a counsellor who had helped me immensely to keep carrying on when things were difficult.

Lastly, I am grateful to my family for always giving me heartfelt support.

References

Adames, Ángel F. and Daehyun Kim, "The MJO as a Dispersive, Convectively Coupled Moisture Wave: Theory and Observations," *J. Atmos. Sci.*, mar 2016, *73* (3), 913–941.

Ashok, Karumuri, Swadhin K. Behera, Suryachandra A. Rao, Hengyi Weng, and Toshio Yamagata, "El Niño Modoki and its possible teleconnection," *J. Geophys. Res.*, nov 2007, *112* (C11), C11007.

Bechtold, Peter, Martin Köhler, Thomas Jung, Francisco Doblas-Reyes, Martin Leutbecher, Mark J. Rodwell, Frederic Vitart, and Gianpaolo Balsamo, "Advances in simulating atmospheric variability with the ECMWF model: From synoptic to decadal time-scales," *Q. J. R. Meteorol. Soc.*, jul 2008, *134* (634), 1337–1351.

Benedict, James J. and David A. Randall, "Structure of the Madden-Julian Oscillation in the Superparameterized CAM," *J. Atmos. Sci.*, nov 2009, *66* (11), 3277–3296.

_ and _ , "Impacts of Idealized Air-Sea Coupling on Madden-Julian Oscillation Structure in the Superparameterized CAM," *J. Atmos. Sci.*, sep 2011, *68* (9), 1990–2008.

_ , Michael S. Pritchard, and William D. Collins, "Sensitivity of MJO propagation to a robust positive Indian Ocean dipole event in the superparameterized CAM," *J. Adv. Model. Earth Syst.*, dec 2015, *7* (4), 1901–1917.

Bretherton, Christopher S., Matthew E. Peters, and Larissa E. Back, "Relationships between water vapor path and precipitation over the tropical oceans," *J. Clim.*, 2004, *17* (7), 1517–1528.

Charney, Jule G., "A Note on Large-Scale Motions in the Tropics," *J. Atmos. Sci.*, nov 1963, *20* (6), 607–609.

Chikira, Minoru and Masahiro Sugiyama, "Eastward-Propagating Intraseasonal Oscillation Represented by Chikira-Sugiyama Cumulus Parameterization. Part I: Comparison with Observation and Reanalysis," *J. Atmos. Sci.*, dec 2013, *70* (12), 3920–3939.

Dee, D. P., S. M. Uppala, A. J. Simmons, P. Berrisford, P. Poli, S. Kobayashi, U. Andrae, M. A. Balmaseda, G. Balsamo, P. Bauer, P. Bechtold, A. C. M. Beljaars, L. van de Berg, J. Bidlot, N. Bormann, C. Delsol, R. Dragani, M. Fuentes, A. J. Geer, L. Haimberger, S. B. Healy, H. Hersbach, E. V. Hólm, L. Isaksen, P. Kållberg, M. Köhler, M. Matricardi, A. P. McNally, B. M. Monge-Sanz, J.-J. Morcrette, B.-K. Park, C. Peubey, P. de Rosnay, C. Tavolato, J.-N. Thépaut, and F. Vitart, "The ERA-Interim reanalysis: configuration and performance of the data assimilation system," *Q. J. R. Meteorol. Soc.*, apr 2011, *137* (656), 553–597.

DeMott, Charlotte A., Cristiana Stan, David A. Randall, and Mark D. Branson, "Intraseasonal Variability in Coupled GCMs: The Roles of Ocean Feedbacks and Model Physics," *J. Clim.*, jul 2014, *27* (13), 4970–4995.

_ , Nicholas P. Klingaman, and Steven J. Woolnough, "Atmosphere-ocean coupled processes in the Madden-Julian oscillation," *Rev. Geophys.*, dec 2015, *53* (4), 1099–1154.

Duchon, Claude E, "Lanczos Filtering in One and Two Dimensions," *J. Appl. Meteorol.*, aug 1979, *18* (8), 1016–1022.

Feng, Jing, Tim Li, Weijun Zhu, Jing Feng, Tim Li, and Weijun Zhu, "Propagating and Nonpropagating MJO Events over Maritime Continent," *J. Clim.*, nov 2015, *28* (21), 8430–8449.

Fieux, Michele and Henry Stommel, "Onset of the Southwest Monsoon over the Arabian Sea from Marine Reports of Surface Winds: Structure and Variability," *Mon. Weather Rev.*, feb 1977, *105* (2), 231–236.

Flatau, Maria, Piotr J. Flatau, Patricia Phoebus, and Pearn P. Niiler, "The Feedback between Equatorial Convection and Local Radiative and Evaporative Processes: The Implications for Intraseasonal Oscillations," *J. Atmos. Sci.*, oct 1997, *54* (19), 2373–2386.

Gates, W. Lawrence, "AMIP: The Atmospheric Model Intercomparison Project," *Bull. Am. Meteorol. Soc.*, dec 1992, *73* (12), 1962–1970.

Gill, A. E., "Some simple solutions for heat-induced tropical circulation," *Q. J. R. Meteorol. Soc.*, jul 1980, *106* (449), 447–462.

Grabowski, Wojciech W., "Coupling Cloud Processes with the Large-Scale Dynamics Using the Cloud-Resolving Convection Parameterization (CRCP)," *J. Atmos. Sci.*, may 2001, *58* (9), 978–997.

Graham, N E and T P Barnett, "Sea Surface Temperature, Surface Wind Divergence, and Convection over Tropical Oceans.," *Science*, oct 1987, *238* (4827), 657–9.

Hannah, Walter M. and Eric D. Maloney, "The moist static energy budget in NCAR CAM5 hindcasts during DYNAMO," *J. Adv. Model. Earth Syst.*, jun 2014, *6* (2), 420–440.

_ , _ , and Michael S. Pritchard, "Consequences of systematic model drift in DYNAMO MJO hindcasts with SP-CAM and CAM5," *J. Adv. Model. Earth Syst.*, sep 2015, *7* (3), 1051–1074.

Hayashi, Yoshikazu, "Frictional Convergence due to Large-Scale Equatorial Waves in a Finite-Depth Ekman Layer," *J.Met.Soc.Japan*, 1971, *49* (6), 450–466.

Hendon, Harry H. and Murry L. Salby, "The Life Cycle of the Madden-Julian Oscillation," *J. Atmos. Sci.*, 1994, *51* (15), 2225–2237.

_ , Chidong Zhang, and John D. Glick, "Interannual variation of the Madden-Julian oscillation during austral summer," *J. Clim.*, 1999, *12* (8 PART 2), 2538–2550.

Hendon, Harry H, Matthew C Wheeler, and Chidong Zhang, "Seasonal Dependence of the MJO-ENSO Relationship," *J. Clim.*, feb 2007, *20* (3), 531–543.

Hirata, Fernando E., Peter J. Webster, and Violeta E. Toma, "Distinct manifestations of austral summer tropical intraseasonal oscillations," *Geophys. Res. Lett.*, jun 2013, *40* (12), 3337–3341.

Inness, Peter M. and Julia M. Slingo, "Simulation of the Madden-Julian oscillation in a coupled general circulation model. Part I: Comparison with observations and an atmosphere-only GCM," *J. Clim.*, feb 2003, *16* (3), 345–364.

_ , _ , Eric Guilyardi, and Jeffrey Cole, "Simulation of the Madden-Julian Oscillation in a Coupled General Circulation Model. Part II: The Role of th e Basic State," *J. Clim.*, feb 2003, *16* (3), 365–382.

Izumo, Takeshi, Sébastien Masson, Jérome Vialard, Clément de Boyer Montegut, Swadhin K. Behera, Gurvan Madec, Keiko Takahashi, and Toshio Yamagata, "Low and high frequency Madden-Julian oscillations in austral summer: interannual variations," *Clim. Dyn.*, sep 2010, *35* (4), 669–683.

Jenkner, Johannes, William W. Hsieh, and Alex J. Cannon, "Seasonal Modulations of the Active MJO Cycle Characterized by Nonlinear Principal Component Analysis," *Mon. Weather Rev.*, jul 2011, *139* (7), 2259–2275.

Jiang, Xianan, Duane E. Waliser, Prince K. Xavier, Jon Petch, Nicholas P. Klingaman, Steven J. Woolnough, Bin Guan, Gilles Bellon, Traute Crueger, Charlotte DeMott, Cecile Hannay, Hai Lin, Wenting Hu, Daehyun Kim, Cara-Lyn Lappen, Mong-Ming Lu, Hsi-Yen Ma, Tomoki Miyakawa, James A. Ridout, Siegfried D. Schubert, John Scinocca, Kyong-Hwan Seo, Eiki Shindo, Xiaoliang Song, Cristiana Stan, Wan-Ling Tseng, Wanqiu Wang, Tongwen Wu, Xiaoqing Wu, Klaus Wyser, Guang J. Zhang, and Hongyan Zhu, "Vertical structure and physical processes of the Madden-Julian oscillation: Exploring key model physics in climate simulations," *J. Geophys. Res. Atmos.*, may 2015, *120* (10), 4718–4748.

Kajikawa, Yoshiyuki, Bin Wang, and Jing Yang, "A multi-time scale Australian monsoon index," *Int. J. Clim.*, 2009, *30* (8), 1114–1120.

Kalnay, E., M. Kanamitsu, R. Kistler, W. Collins, D. Deaven, L. Gandin, M. Iredell, S. Saha, G. White, J. Woollen, Y. Zhu, A. Leetmaa, R. Reynolds, M. Chelliah,

W. Ebisuzaki, W. Higgins, J. Janowiak, K. C. Mo, C. Ropelewski, J. Wang, Roy Jenne, and Dennis Joseph, "The NCEP/NCAR 40-Year Reanalysis Project," *Bull. Am. Meteorol. Soc.*, mar 1996, *77* (3), 437–471.

Kikuchi, Kazuyoshi, "An introduction to combined Fourier-wavelet transform and its application to convectively coupled equatorial waves," *Clim. Dyn.*, sep 2014, *43* (5-6), 1339–1356.

_ **, Bin Wang, and Yoshiyuki Kajikawa**, "Bimodal representation of the tropical intraseasonal oscillation," *Clim. Dyn.*, may 2012, *38* (9-10), 1989–2000.

_ **, Chihiro Kodama, Tomoe Nasuno, Masuo Nakano, Hiroaki Miura, Masaki Satoh, Akira T. Noda, and Yohei Yamada**, "Tropical intraseasonal oscillation simulated in an AMIP-type experiment by NICAM," *Clim. Dyn.*, apr 2017, *48* (7-8), 2507–2528.

Kiladis, George N., Juliana Dias, Katherine H. Straub, Matthew C. Wheeler, Stefan N. Tulich, Kazuyoshi Kikuchi, Klaus M. Weickmann, and Michael J. Ventrice, "A Comparison of OLR and Circulation-Based Indices for Tracking the MJO," *Mon. Weather Rev.*, dec 2013, *142* (5), 1697–1715.

Kim, Daehyun, Adam H. Sobel, Eric D. Maloney, Dargan M. W. Frierson, and In-Sik Kang, "A Systematic Relationship between Intraseasonal Variability and Mean State Bias in AGCM Simulations," *J. Clim.*, nov 2011, *24* (21), 5506–5520.

_ **, Jong Seong Kug, and Adam H. Sobel**, "Propagating versus nonpropagating Madden-Julian oscillation events," *J. Clim.*, 2014, *27* (1), 111–125.

Kim, Hye-Mi, Daehyun Kim, Frederic Vitart, Violeta E. Toma, Jong-Seong Kug, and Peter J. Webster, "MJO Propagation across the Maritime Continent in the ECMWF Ensemble Prediction System," *J. Clim.*, jun 2016, *29* (11), 3973–3988.

Kim, Seon Tae, Jin-Yi Yu, and Mong-Ming Lu, "The distinct behaviors of Pacific and Indian Ocean warm pool properties on seasonal and interannual time scales," *J. Geophys. Res. Atmos.*, 2012, *117* (D5), D05128.

Kiranmayi, L. and Eric D. Maloney, "Intraseasonal moist static energy budget in reanalysis data," *J. Geophys. Res. Atmos.*, 2011, *116* (21), 1–12.

Klingaman, N. P. and S. J. Woolnough, "The role of air-sea coupling in the simulation of the Madden-Julian oscillation in the Hadley Centre model," *Q. J. R. Meteorol. Soc.*, oct 2014, *140* (684), 2272–2286.

Knutson, Thomas R., Klaus M. Weickmann, and Thomas R. Knutson, "30-60 Day Atmospheric Oscillations: Composite Life Cycles of Convection and Circulation Anomalies," *Mon. Weather Rev.*, jul 1987, *115* (7), 1407–1436.

Kodama, Chihiro, Yohei Yamada, Akira T. Noda, Kazuyoshi Kikuchi, Yoshiyuki Kajikawa, Tomoe Nasuno, Tomohiko Tomita, Tsuyoshi Yamaura, Hiroshi G. Takahashi, Masayuki Hara, Yoshio Kawatani, Masaki Satoh, and Masato Sugi, "A 20-Year Climatology of a NICAM AMIP-Type Simulation," *J. Meteorol. Soc. Japan. Ser. II*, 2015, *93* (4), 393–424.

Liebmann, B and CA Smith, "Description of a complete (interpolated) outgoing longwave radiation dataset," *Bull. Amer. Met. Soc.*, 1996, *77*, 1275–1277.

Lindzen, Richard S. and Sumant Nigam, "On the Role of Sea Surface Temperature Gradients in Forcing Low-Level Winds and Convergence in the Tropics," *J. Atmos. Sci.*, sep 1987, *44* (17), 2418–2436.

Ling, Jian, Chongyin Li, Wen Zhou, and Xiaolong Jia, "To begin or not to begin? A case study on the MJO initiation problem," *Theor. Appl. Climatol.*, 2013, *115* (1-2), 231–241.

Madden, Roland A. and Paul R. Julian, "Detection of a 40-50 Day Oscillation in the Zonal Wind in the Tropical Pacific," *J. Atmos. Sci.*, jul 1971, *28* (5), 702–708.

_ and _, "Description of Global-Scale Circulation Cells in the Tropics with a 40-50 Day Period," *J. Atmos. Sci.*, sep 1972, *29* (6), 1109–1123.

Majda, Andrew J and Samuel N Stechmann, "The skeleton of tropical intraseasonal oscillations.," *Proc. Natl. Acad. Sci. U. S. A.*, 2009, *106* (21), 8417–22.

Maloney, Eric D. and Dennis L. Hartmann, "The Sensitivity of Intraseasonal Variability in the NCAR CCM3 to Changes in Convective Parameterization," *J. Clim.*, may 2001, *14* (9), 2015–2034.

Masunaga, Hirohiko, "Seasonality and Regionality of the Madden-Julian Oscillation, Kelvin Wave, and Equatorial Rossby Wave," *J. Atmos. Sci.*, dec 2007, *64* (12), 4400–4416.

Matsuno, T., "Quasi-geostrophic motions in the equatorial area," *J. Meteorol. Soc. Japan*, 1966, *44*, 25–42.

Matthews, Adrian J., "Primary and successive events in the Madden-Julian Oscillation," *Q. J. R. Meteorol. Soc.*, jan 2008, *134* (631), 439–453.

Milliff, Ralph F. and Roland A. Madden, "The Existence and Vertical Structure of Fast, Eastward-Moving Disturbances in the Equatorial T roposphere," *J. Atmos. Sci.*, feb 1996, *53* (4), 586–597.

Miura, H., T. Suematsu, and T. Nasuno, "An ensemble hindcast of the Madden-Julian oscillation during the CINDY2011/DYNAMO field campaign and influence of seasonal variation of sea surface temperature," *J. Meteorol. Soc. Japan*, 2016, *93A*.

Miura, Hiroaki, Masaki Satoh, and Masaki Katsumata, "Spontaneous onset of a Madden-Julian oscillation event in a cloud-system-resolving simulation," *Geophys. Res. Lett.*, jul 2009, *36* (13), L13802.

_ , _ , Tomoe Nasuno, Akira T. Noda, and Kazuyoshi Oouchi, "A Madden-Julian Oscillation Event Realistically Simulated by a Global Cloud-Resolving Model," *Science (80-.).*, dec 2007, *318* (5857), 1763–1765.

Miyakawa, Tomoki, Masaki Satoh, Hiroaki Miura, Hirofumi Tomita, Hisashi Yashiro, Akira T. Noda, Yohei Yamada, Chihiro Kodama, Masahide Kimoto, and Kunio Yoneyama, "Madden-Julian Oscillation prediction skill of a new-generation global model demonstrated using a supercomputer," *Nat. Commun.*, may 2014, *5*.

Moum, James N., Kandaga Pujiana, Ren-Chieh Lien, and William D. Smyth, "Ocean feedback to pulses of the Madden-Julian Oscillation in the equatorial Indian Ocean," *Nat. Commun.*, oct 2016, *7*, 13203.

Nakazawa, Tetsuo, "Tropical Super Clusters within Intraseasonal Variations over the Western Pacific," *J. Meteorol. Soc. Japan. Ser. II*, 1988, *66* (6), 823–839.

Neelin, J. David and Isaac M. Held, "Modeling Tropical Convergence Based on the Moist Static Energy Budget," *Mon. Weather Rev.*, 1987, *115* (1), 3–12.

Nishimoto, Eriko and Masato Shiotani, "Intraseasonal variations in the tropical tropopause temperature revealed by cluster analysis of convective activity," *J. Geophys. Res. Atmos.*, may 2013, *118* (9), 3545–3556.

Nitta, Tsuyoshi, Takanori Mizuno, and Kiyotoshi Takahashi, "Multi-Scale Convective Systems during the Initial Phase of the 1986/87 El Niño," *J. Meteorol. Soc. Japan. Ser. II*, feb 1992, *70* (1B), 447–466.

Pohl, Benjamin and Adrian J. Matthews, "Observed Changes in the Lifetime and Amplitude of the Madden-Julian Oscillation Associated with Interannual ENSO Sea Surface Temperature Anomalies," *J. Clim.*, feb 2007, *20* (11), 2659–2674.

Rayner, N. A., D. E. Parker, E. B. Horton, C. K. Folland, L. V. Alexander, D. P. Rowell, E. C. Kent, and A. Kaplan, "Global analyses of sea surface temperature, sea ice, and night marine air temperature since the late nineteenth century," *J. Geophys. Res.*, 2003, *108* (D14), 4407.

Reynolds, Richard W., Nick A. Rayner, Thomas M. Smith, Diane C. Stokes, and Wanqiu Wang, "An Improved In Situ and Satellite SST Analysis for Climate," *J. Clim.*, jul 2002, *15* (13), 1609–1625.

Rui, Hualan and Bin Wang, "Development Characteristics and Dynamic Structure of Tropical Intraseasonal Convection Anomalies," *J. Atmos. Sci.*, feb 1990, *47* (3), 357–379.

Saji, N. H., B. N. Goswami, P. N. Vinayachandran, and T. Yamagata, "A dipole mode in the tropical Indian Ocean," *Nature*, sep 1999, *401* (6751), 360–363.

_ **, S.-P. Xie, and C.-Y. Tam**, "Satellite observations of intense intraseasonal cooling events in the tropical south Indian Ocean," *Geophys. Res. Lett.*, 2006, *33* (14), L14704.

Salby, Murry L. and Harry H. Hendon, "Intraseasonal Behavior of Clouds, Temperature, and Motion in the Tropics," *J. Atmos. Sci.*, aug 1994, *51* (15), 2207–2224.

Satoh, M., T. Matsuno, H. Tomita, H. Miura, T. Nasuno, and S. Iga, "Nonhydrostatic icosahedral atmospheric model (NICAM) for global cloud resolving simulations," *J. Comput. Phys.*, mar 2008, *227* (7), 3486–3514.

Shinoda, Toshiaki and Weiqing Han, "Influence of the Indian Ocean Dipole on Atmospheric Subseasonal Variability," *J. Clim.*, sep 2005, *18* (18), 3891–3909.

_ **, Harry H. Hendon, and John Glick**, "Intraseasonal Variability of Surface Fluxes and Sea Surface Temperature in the Tropical Western Pacific and Indian Oceans," *J. Clim.*, jul 1998, *11* (7), 1685–1702.

Slingo, J. M., D. P. Rowell, K. R. Sperber, and F. Nortley, "On the predictability of the interannual behaviour of the Madden-Julian oscill ation and its relationship with el Niño," *Q. J. R. Meteorol. Soc.*, jan 1999, *125* (554), 583–609.

Sobel, Adam and Eric Maloney, "An Idealized Semi-Empirical Framework for Modeling the Madden-Julian Oscillation," *J. Atmos. Sci.*, 2012, *69* (5), 1691–1705.

_ **and** _ , "Moisture Modes and the Eastward Propagation of the MJO," *J. Atmos. Sci.*, jan 2013, *70* (1), 187–192.

Sobel, Adam H., Johan Nilsson, and Lorenzo M. Polvani, "The Weak Temperature Gradient Approximation and Balanced Tropical Moisture Waves," *J. Atmos. Sci.*, dec 2001, *58* (23), 3650–3665.

Sobel, Adam, Shuguang Wang, and Daehyun Kim, "Moist Static Energy Budget of the MJO during DYNAMO," *J. Atmos. Sci.*, nov 2014, *71* (11), 4276–4291.

Stachnik, Justin P., Duane E. Waliser, and Andrew J. Majda, "Precursor Environmental Conditions Associated with the Termination of Madden-Julian Oscillation Events," *J. Atmos. Sci.*, may 2015, *72* (5), 1908–1931.

Straub, Katherine H., "MJO Initiation in the Real-Time Multivariate MJO Index," *J. Clim.*, sep 2013, *26* (4), 1130–1151.

Takasuka, Daisuke, Tomoki Miyakawa, Masaki Satoh, and Hiroaki Miura, "Topographical Effects on Internally Produced MJO-Like Disturbances in an Aqua-Planet Version of NICAM," *SOLA*, 2015, *11* (0), 170–176.

Takayabu, Yukari N., "Large-Scale Cloud Disturbances Associated with Equatorial Waves," *J. Meteorol. Soc. Japan. Ser. II*, 1994, *72* (3), 433–449.

Tomita, H., H. Miura, S. Iga, T. Nasuno, and M. Satoh, "A global cloud-resolving simulation: Preliminary results from an aqua planet experiment," *Geophys. Res. Lett.*, 2005, *32* (8), L08805.

Tomita, Hirofumi and Masaki Satoh, "A new dynamical framework of nonhydrostatic global model using the icosahedral grid," *Fluid Dyn. Res.*, jun 2004, *34* (6), 357–400.

Trenberth, Kevin E., "The Definition of El Niño," *Bull. Am. Meteorol. Soc.*, dec 1997, *78* (12), 2771–2777.

Waliser, Duane E. and Nicholas E. Graham, "Convective cloud systems and warm-pool sea surface temperatures: Coupled interactions and self-regulation," *J. Geophys. Res.*, 1993, *98* (D7), 12881.

Wang, B and H Rui, "Synoptic climatology of transient tropical intraseasonal convection anomalies: 1975-1985," *Meteorol. Atmos. Phys.*, mar 1990, *44* (1-4), 43–61.

Weickmann, K M and S J S Khalsa, "The Shift of Convection from the Indian Ocean to the Western Pacific Ocean during a 30-60 Day Oscillation," *Mon. Weather Rev.*, apr 1990, *118* (4), 964–978.

Weickmann, Klaus M, Glenn R Lussky, and John E Kutzbach, "Intraseasonal (30-60 Day) Fluctuations of Outgoing Longwave Radiation and 250 mb Streamfunction during Northern Winter," *Mon. Weather Rev.*, jun 1985, *113* (6), 941–961.

Weng, Hengyi, Karumuri Ashok, Swadhin K. Behera, Suryachandra A. Rao, and Toshio Yamagata, "Impacts of recent El Niño Modoki on dry/wet conditions in the Pacific rim during boreal summer," *Clim. Dyn.*, jun 2007, *29* (2-3), 113–129.

Wheeler, Matthew and George N. Kiladis, "Convectively Coupled Equatorial Waves: Analysis of Clouds and Temperature in the Wavenumber-Frequency Domain," *J. Atmos. Sci.*, feb 1999, *56* (3), 374–399.

_ **and Klaus M Weickmann**, "Real-Time Monitoring and Prediction of Modes of Coherent Synoptic to Intraseasonal Tropical Variability," *Mon. Weather Rev.*, nov 2001, *129* (11), 2677–2694.

Wheeler, Matthew C. and Harry H. Hendon, "An All-Season Real-Time Multivariate MJO Index: Development of an Index for Monitoring and Prediction," *Mon. Weather Rev.*, 2004, *132* (8), 1917–1932.

Wilson, Earle A., Arnold L. Gordon, and Daehyun Kim, "Observations of the Madden Julian Oscillation during Indian Ocean Dipole events," *J. Geophys. Res. Atmos.*, mar 2013, *118* (6), 2588–2599.

Wyrtki, K., "Some thoughts about the west Pacific warm pool," in Thierry Picaut, Joël and Lukas, Roger B. and Delcroix, ed., *Thierry Picaut, Joël and Lukas, Roger B. and Delcroix, ed.*, Western Pacific International Meeting and Workshop on Toga Coare, Nouméa 1989, pp. 99–110.

Yasunaga, Kazuaki, "Seasonality and Regionality of the Madden-Julian Oscillation and Convectively Coupled Equatorial Waves," *SOLA*, 2011, *7*, 153–156.

Yoshizaki, Masanori, Kazuaki Yasunaga, Shin ichi Iga, Masaki Satoh, Tomoe Nasuno, Akira T. Noda, and Hirofumi Tomita, "Why do Super Clusters and Madden Julian Oscillation Exist over the Equatorial Region?," *SOLA*, 2012, *8*, 33–36.

Zhang, Chidong, "Large-Scale Variability of Atmospheric Deep Convection in Relation to Sea Surface Temperature in the Tropics," *J. Clim.*, oct 1993, *6* (10), 1898–1913.

_ , "Madden-Julian Oscillation," *Rev. Geophys.*, jun 2005, *43* (2), RG2003.

_ , "Madden-Julian Oscillation: Bridging Weather and Climate," *Bull. Am. Meteorol. Soc.*, apr 2013, *94* (12), 1849–1870.

_ **and Jian Ling**, "Barrier Effect of the Indo-Pacific Maritime Continent on the MJO: Perspectives from Tracking MJO Precipitation," *J. Clim.*, may 2017, *30* (9), 3439–3459.

_ **and Jonathan Gottschalck**, "SST Anomalies of ENSO and the Madden-Julian Oscillation in the Equatorial Pacific," *J. Clim.*, sep 2002, *15* (17), 2429–2445.

_ **and Min Dong**, "Seasonality in the Madden-Julian Oscillation," *J. Clim.*, aug 2004, *17* (16), 3169–3180.

Zhu, Jieshun, Wanqiu Wang, and Arun Kumar, "Simulations of MJO Propagation across the Maritime Continent: Impacts of SST Feedback," *J. Clim.*, mar 2017, *30* (5), 1689–1704.